Technology

Molecular Cell

# ATAC-Me Captures Prolonged DNA Methylation of Dynamic Chromatin Accessibility Loci during Cell Fate Transitions

## Graphical Abstract

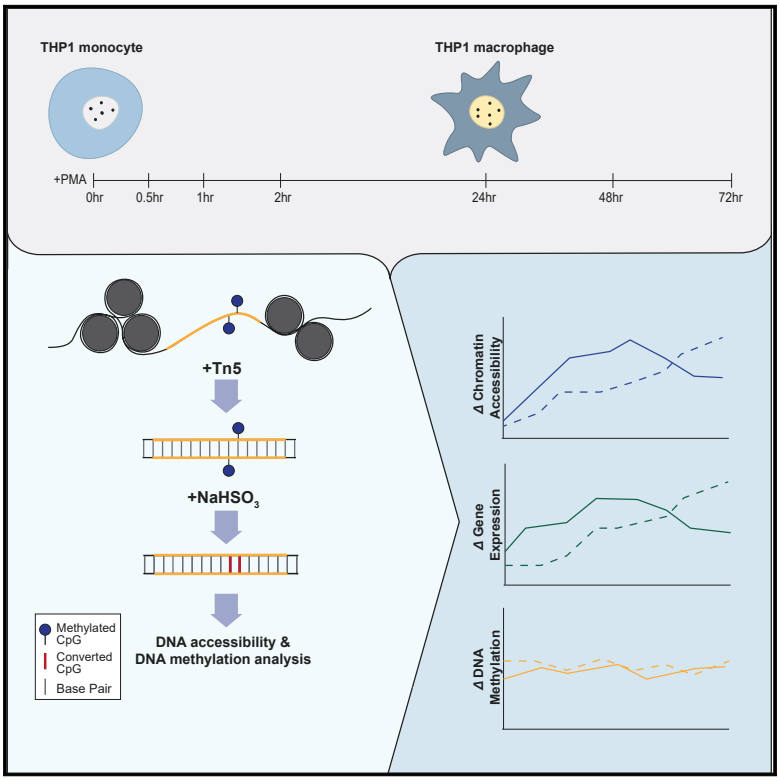


## Highlights

- ATAC-Me simultaneously measures chromatin accessibility and DNA methylation (DNAme)
- Enhancer accessibility and DNAme change independently during cell fate transitions
- Loss of DNAme is delayed in nascent open chromatin regions
- Transcriptional changes track with new enhancer accessibility despite prolonged DNAme

## Authors

Kelly R. Barnett, Benjamin E. Decato, Timothy J. Scott, ..., Jonathan Attalla, Andrew D. Smith, Emily Hodges

## Correspondence

emily.hodges@vanderbilt.edu

## In Brief

Barnett et al. describe ATAC-Me, an approach that captures chromatin accessibility and DNA methylation simultaneously from a single DNA fragment library. ATAC-Me was used to probe temporal relationships between epigenetic and gene regulatory changes at enhancers during myeloid differentiation of THP1 monocytes, revealing a decoupling of chromatin and DNA methylation changes at transitioning enhancers.

Barnett et al., 2020, Molecular Cell 77, 1–15
March 19, 2020 
https://doi.org/10.1016/j.molcel.2020.01.004

CellPress

Please cite this article in press as: Barnett et al., ATAC-Me Captures Prolonged DNA Methylation of Dynamic Chromatin Accessibility Loci during Cell Fate Transitions, Molecular Cell (2020), https://doi.org/10.1016/j.molcel.2020.01.004

Molecular Cell
Technology

# ATAC-Me Captures Prolonged DNA Methylation of Dynamic Chromatin Accessibility Loci during Cell Fate Transitions

Kelly R. Barnett,[1] Benjamin E. Decato,[2] Timothy J. Scott,[1] Tyler J. Hansen,[1] Bob Chen,[1] Jonathan Attalla,[1] Andrew D. Smith,[2] and Emily Hodges[1,3,*]
[1]Department of Biochemistry and Vanderbilt Genetics Institute, Vanderbilt University School of Medicine, Nashville, TN 37232, USA
[2]Quantitative and Computational Biology, Department of Biological Sciences, University of Southern California, Los Angeles, CA 90089, USA
[3]Lead Contact
*Correspondence: emily.hodges@vanderbilt.edu
https://doi.org/10.1016/j.molcel.2020.01.004

## SUMMARY

**DNA methylation of enhancers is dynamic, cell-type specific, and vital for cell fate progression. However, current models inadequately define its role within the hierarchy of gene regulation. Analysis of independent datasets shows an unanticipated overlap between DNA methylation and chromatin accessibility at enhancers of steady-state stem cells, suggesting that these two opposing features might exist concurrently. To define their temporal relationship, we developed ATAC-Me, which probes accessibility and methylation from single DNA library preparations. We identified waves of accessibility occurring rapidly across thousands of myeloid enhancers in a monocyte-to-macrophage cell fate model. Prolonged methylation states were observed at a majority of these sites, while transcription of nearby genes tracked closely with accessibility. ATAC-Me uncovers a significant disconnect between chromatin accessibility, DNA methylation status, and gene activity. This unexpected observation highlights the value of ATAC-Me in constructing precise molecular timelines for understanding the role of DNA methylation in gene regulation.**

## INTRODUCTION

Integrative analysis of epigenomic data has identified a range of enhancer states across diverse cell types and their developmental intermediates (Ernst and Kellis, 2012). Certain classes of enhancers (active, repressed, poised) feature distinct combinations of histone modifications (Rada-Iglesias et al., 2012; Zentner et al., 2011) and chromatin accessibility (ChrAcc) patterns (Thurman et al., 2012). Such combinations may represent stages in the stepwise process of gene regulation coordinated by transcription factor (TF) DNA-binding events. This intimate temporal relationship between the epigenome and TFs is thought to ensure proper orchestration of TF activity and is critical for normal specification of cellular function and phenotype (Heinz et al., 2010).

DNA methylation (DNAme) in particular is thought to stabilize cellular identity in the context of gene regulation (Schübeler, 2015). DNAme is typically associated with stable repression of promoters and enhancers, while hypo- or low DNAme reflects past or present occupancy of gene-regulatory elements (GREs) by factors involved in transcriptional control (Hodges et al., 2011; Jadhav et al., 2019; Lister et al., 2009; Stadler et al., 2011). Although DNAme is indispensable for proper cellular differentiation and gene activation (Dawlaty et al., 2014; Okano et al., 1999), current models of enhancer dynamics only weakly describe a role for DNAme within this ordered process. Furthermore, the degree to which DNAme influences enhancer regulation of gene transcription is unclear.

Comparative analysis of genome-wide DNAme datasets from diverse tissues has shown that the degree of differential methylation between cell types is much greater in distal GREs outside of CpG island promoters (Bock et al., 2012; Hodges et al., 2011; Stadler et al., 2011). These patterns of DNAme are characterized by local, cell type-specific hotspots of CpG hypomethylation often overlapping enhancer histone marks and DNase hypersensitive sites. We have previously suggested that combined signatures of DNAme and ChrAcc may reflect stages of enhancer activation (Schlesinger et al., 2013). Our analysis of steady-state data revealed that DNAme and ChrAcc co-occur across a surprising number of sites in pluripotent stem cells. In mature cells, this duality is seemingly resolved by further loss of methylation (active) or loss of accessibility (repressed), suggesting that DNAme changes are, perhaps not surprisingly, sequential to nucleosome repositioning during enhancer activation. Indeed, several recent studies support a model in which inaccessible enhancers are primed by pioneer TFs, leading to chromatin remodeling, increased ChrAcc, and concomitant loss of DNAme (Donaghey et al., 2018; Mayran et al., 2018). On the basis of this and other observations, we hypothesized that these dual states may indicate a unique stage along the enhancer regulation continuum and that loss of methylation during cell fate transitions is a final, necessary step in the process of enhancer activation and thus the establishment or stabilization of cell identity.

The ability to test this model, however, has been limited in part by a lack of molecular tools to measure spatiotemporal relationships at high resolution on a genome-wide scale and, most important, directly within the context of chromatin. Consequently, our genome-scale understanding of relationships between DNAme and other aspects of enhancer regulation is based on disconnected datasets derived from steady-state, asynchronous cell populations or time point-associated datasets too far removed from one another to capture transient cellular states. To better characterize the spatiotemporal relationship between ChrAcc and DNAme, we developed an approach that enables simultaneous measurement of these two distinct biochemical events from the same population of DNA molecules. Our approach, aptly named ATAC-Me, is an adaptation of two techniques combining transposase-assisted enrichment of ChrAcc fragments from native chromatin (Buenrostro et al., 2013) with subsequent sodium bisulfite conversion and deep sequencing (Adey and Shendure, 2012; Wang et al., 2013).

We performed ATAC-Me, RNA sequencing (RNA-seq), and reference-point whole-genome bisulfite sequencing (WGBS) on a densely sampled time course of PMA (phorbol 12-myristate 13-acetate)-induced THP-1 monocytes differentiated to macrophages. Our approach reveals ChrAcc and DNAme may be quantitatively decoupled at myeloid enhancers as they appear to become poised, active, or repressed during early monocyte-to-macrophage transitions. We observed persistent hypermethylation of an unexpected number of DNA fragments derived from nascent ChrAcc regions, corroborating earlier observations that potentially transient states coexist (Schlesinger et al., 2013). At early time points (0–24 h), dynamic ChrAcc regions were associated with a range of seemingly inert DNAme states, yet robust transcriptional responses of neighboring genes were observed, suggesting that DNAme does not immediately affect gene-regulatory responses. Minimal loss of DNAme was observed at later time points (48 and 72 h), and dramatic DNAme changes were observed only with the application of an artificial DNA demethylation stimulus (L-ascorbic acid 2-phosphate [L-AA-2-P]), suggesting a secondary consequential role for DNAme removal at GREs. Ultimately these studies are critical to disentangle the role of DNAme dynamics in normal cellular differentiation.

## Design

To better elucidate spatiotemporal relationships between ChrAcc and DNAme, we required an approach that would capture both ChrAcc and DNAme from the same population of DNA molecules. Comparable approaches have been described (Kelly et al., 2012; Li and Tollefsbol, 2011), but these methodologies are technically prohibitive and limited in their ability to provide the resolution and coverage required to study dynamic enhancer regions. We required a sequence-independent strategy (not reliant on specific recognition sites of enzymes), with the ability to directly probe the methylation status of accumulating ChrAcc fragments at transitioning enhancers. Because of its simple, cost-effective protocol and low input requirement, ATAC-seq (assay for transposase accessible chromatin) has become a widely adopted method for profiling ChrAcc regions genome-wide. In our adaptation of the approach, Tn5-enriched ChrAcc fragments are further subjected to sodium bisulfite conversion of unmethylated cytosines before library amplification and sequencing (Figure 1A).

Preserving the fidelity of DNAme states during ATAC-Me library construction was crucial to this study. There are known opportunities during bisulfite library construction when the information content of the original DNA fragment can become artificially overwritten. Prior approaches for constructing WGBS libraries with Tn5-based methodologies have used a conservative end-repair step involving gap filling and nick ligation to produce bisulfite converted, Illumina sequencing-competent DNA libraries (Adey and Shendure, 2012; Wang et al., 2013). Alternative efforts to streamline bisulfite adaptation of Tn5 protocols have used an extension-based approach to create sequencing compatible libraries (Lu et al., 2015; Spektor et al., 2019; Suzuki et al., 2018). Specifically, an initial tagmentation with Tn5 transposomes assembled with asymmetric, methylated adapters is followed by a polymerase extension step with a 5-methyl-deoxycytidine (5-methyl-dCTP) nucleotide tri-phosphate blend. With fewer molecular steps required, this approach would simplify ATAC-Me library construction; however, several studies have reported detectable levels of exogenous cytosine methylation in the tagmented genomic DNA, effectively creating false methylation signals (Lu et al., 2015; Suzuki et al., 2018).

Taking advantage of *Drosophila melanogaster* genomic DNA (S2 cells), which is devoid of DNAme (Dunwell and Pfeifer, 2014), we compared the gap filling and nick ligation approach with the extension approach. Analysis of nucleotide base composition across reads from different bisulfite library construction conditions indicated that in all replicates and conditions of extension-based approaches, cytosine signal was detected (Figures S1A and S1B). In contrast, a gap filling (using a 5-methyl-dCTP-substituted NTP mix) and nick ligation approach produced the expected nucleotide base composition profile of bisulfite converted *Drosophila* DNA, virtually devoid of cytosine signal. Analysis of individual CpG methylation levels revealed methylation frequencies greater than 10% for extension-based libraries compared with DNAme levels seen by gap filling and nick ligation with or without 5-methyl-dCTP. Exogenous levels of methylation even at low levels could potentially confound our data; therefore we opted to perform gap filling and nick ligation-based ATAC-Me.

Assessing the spatiotemporal relationship between ChrAcc and DNAme requires a dynamic, rather than steady-state, cellular system. Approaches are not yet feasible that capture these relationships in real time. Thus, we are required to sample DNA fragments at sequential time points, and the selection of those time points is an important component to our approach. To test our method, we chose THP-1 cells, a well-established model system for studying inflammatory responses *in vitro* (Tsuchiya et al., 1982). THP-1s originate from a monocytic leukemia that, upon relatively short exposure to various stimuli including PMA, can be differentiated into naive M(−) macrophages. In addition, these cells exhibit exceptionally low phenotypic heterogeneity, an important consideration when measuring epigenetic states from cell populations.

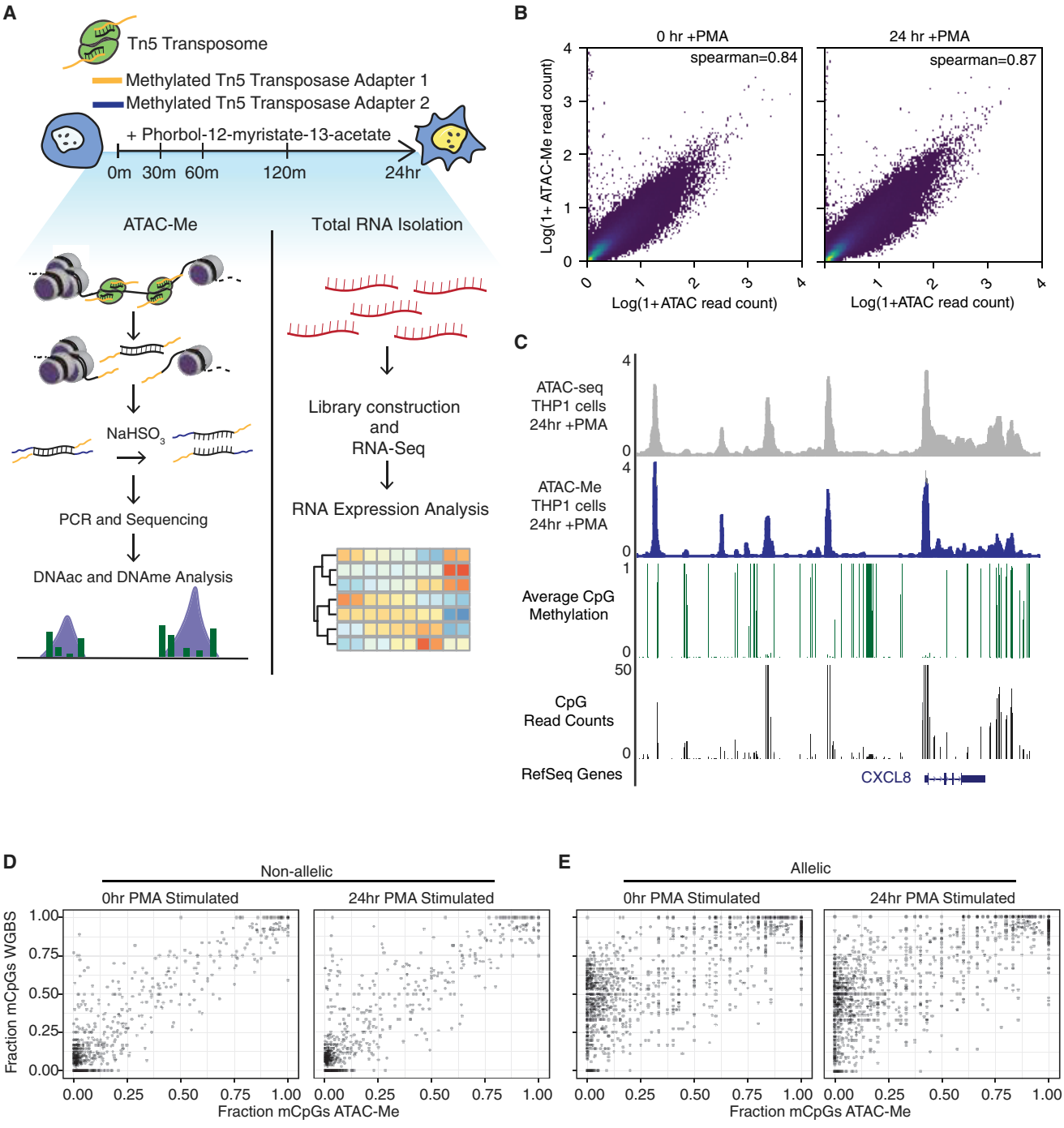


**Figure 1. ATAC-Me Accurately Measures the Chromatin-Accessible Methylome**

(A) Methodology overview of ATAC-Me library construction and experimental design.

(B). Spearman rank comparison of standard ATAC and ATAC-Me read counts at 0 or 24 h PMA stimulation within a common set of broad peak accessible regions.

(C) Genome Browser profile of the *CXCL8* locus displaying ATAC-seq accessibility signal (gray), ATAC-Me accessibility signal (blue), CpG methylation frequency (green), and CpG read abundance (black). All data shown have been read depth normalized.

(D) Scatterplot of mCpG fraction in THP-1 cells calculated with WGBS or ATAC-Me data for CpGs in non-allelicly regulated regions (Pearson r = 0.92, $p < 0.0001$, 0 h; Pearson r = 0.91, $p < 0.0001$, 24 h).

(E) CpGs within validated allele-specific methylated (Pearson r = 0.80, $p < 0.0001$, 0 h; Pearson r = 0.80, $p < 0.0001$, 24 h) regions. The CpG subset that displayed the expected intermediate methylation state for allelicly regulated region (ARR) CpGs as calculated from WGBS data was not correlated with ATAC-Me CpG methylation (Pearson r = 0.02, p = 0.59, 0 h; Pearson r = 0.02, p = 0.64, 24 h).

See also Figures S1–S3.

Nuclear run-on sequencing studies, which map RNA polymerase activity at enhancers, have demonstrated that the immediate effects of TF signaling can occur within as little as 15 min upon stimulation (Hah et al., 2011). In addition, PMA is a robust stimulus at the applied concentration (100 ng/mL, 162 nM), as evident by a visual increase in cell adhesion in as little as 0.5 h. Therefore, we expect an immediate and primary gene-regulatory response to PMA followed by a secondary more stable gene-regulatory response specific to the macrophage transition. Given these considerations, we initially performed ATAC-Me on cells collected at 0, 0.5, 1, and 2 h, as well as 24 h, following PMA stimulation in order to capture both immediate and subsequent gene-regulatory responses. In parallel, we collected RNA for each time point (Figure 1A) in addition to standard ATAC-seq and WGBS data for key reference time points (0 and 24 h). To validate our time course, we confirmed from RNA-seq data the upregulation of known markers of PMA-induced macrophage differentiation as early as 0.5 h post-PMA treatment (Figure S1C).

## RESULTS

### ATAC-Me Is Reproducible and Recapitulates Standard ATAC-Seq

Bisulfite treatment is known to be detrimental to DNA integrity, potentially leading to loss of material and erosion of the typical ATAC-seq fragment size distribution. When comparing fragment size distributions for ATAC-Me with standard ATAC, we observe a distinct loss of material, but the DNA fragment size range (<130 bp) most enriched for chromatin-accessible fragments is preserved with the greatest fragment losses representing mono-, di-, and tri-nucleosome fragments (Figures S2A–S2D). Nevertheless, distinct mono-nucleosome signal can be observed within the ATAC-Me size distribution, indicating that nucleosome patterns proximal to open chromatin peaks are preserved to some extent.

We used MACS2 to determine ATAC-Me peak locations genome-wide, detecting on average 57,217 high-confidence, reproducible peaks across all time points in accordance with ChrAcc peak estimates from earlier ATAC-seq studies (Buenrostro et al., 2013). Only peak regions reproducible in both individual and merged ATAC-Me replicates were selected for analysis. We compared the performance of ATAC-Me with that of standard ATAC-seq, generating libraries in parallel and in duplicate from the same population of time point-specific nuclei (0 and 24 h). Initial comparisons of peak calls between the two methodologies demonstrated that more than 75% of peak regions in standard ATAC-seq were replicated by the paired ATAC-Me dataset (Figures S2E and S2F). Furthermore, we observed high concordance between peak signals in both datasets as well as between replicates (Figures 1B and 1C; Figure S3). Whereas twice the number of peaks is called in ATAC-Me versus standard ATAC-seq, manual and global comparison of read counts at ATAC-Me only peak regions reveals high correspondence between ATAC-Me and standard ATAC-seq (Figures S2G–S2J), indicating the discrepancy in peak calling is likely due to differences in local background estimates used by the peak calling algorithm, as discussed previously (Zhang et al., 2008).

### ATAC-Me Accurately Profiles the Methylome of Open Chromatin

Using ATAC-Me, we measured methylation at all CpG sites located within Tn5-enriched DNA fragments for every time point collected. In parallel, we performed tagmentation-based WGBS on genomic DNA collected at 0 and 24 h in order to create gold-standard references for methylation of both endpoints (Figures 1D and 1E). We compared ATAC-Me and WGBS methylation distributions within ChrAcc peak regions identified at 0 and 24 h. As expected, methylation levels of ATAC-Me and WGBS are largely concordant within peak regions and extensively hypomethylated compared with the bimodal distribution of methylation levels typically observed in WGBS (Figure 1D).

WGBS data represent an average measurement of DNAme without consideration of the actual *in cellulo* accessibility of DNA fragments. For instance, allelicly regulated regions (ARRs) are known to consist of one hypomethylated, chromatin-accessible allele and one hypermethylated, inaccessible allele (Martos et al., 2017; Shibata et al., 1996; Stern et al., 2017), which would be 50% methylated according to WGBS. Accordingly, our ATAC-Me methodology should selectively enrich for the chromatin-accessible, hypomethylated allele within these ARRs compared with WGBS. To determine the specificity of ATAC-Me to measure methylation of accessible DNA, we compared methylation levels of known ARRs, including imprinting control regions (Fang et al., 2012). Indeed, we detected significantly lower methylation levels of ARRs profiled by ATAC-Me compared with those measured by WGBS (Figure 1E). The implications of these observations are that (1) ATAC-Me is highly selective for accessible DNA fragments, offering a more incisive view of methylation states within the context of chromatin compared with WGBS, and (2) observed methylation of accessible fragments is not due to random noise.

In general, ATAC-Me CpG methylation levels within steady-state, ChrAcc regions are highly concordant with WGBS. However, outside of defined peak regions, low-level noise resulting from molecular "breathing" of histone-bound DNA as well as spurious exposure of DNA to Tn5 transposase results in low read coverage of select CpGs within inaccessible chromatin regions where DNAme may be determined with some accuracy (Figure 1C). Comparison of ATAC-Me read "noise" outside defined peak regions with WGBS data revealed a surprisingly high level of concordance despite locally minimal read depth in these "no peak" regions (Figure S4A), thus demonstrating further utility for ATAC-Me to partially interrogate the DNAme state of long stretches of inaccessible chromatin.

Overall, ATAC-Me uniquely permits methylation of accessible chromatin regions to be determined, where TFs and other proteins are known to interact with DNA, thus providing enhanced biological context to DNAme patterns compared with traditional WGBS. As sequence coverage is highly focused on accessible DNA fragments, probing DNAme of relevant targets requires less sequencing than orthogonal methodologies. Similar to restriction enzyme-based methods (enhanced reduced representation bisulfite sequencing [ERRBS]; Akalin et al., 2012), the approach is essentially a selective representation of the methylome; yet, unlike reduced representation bisulfite sequencing (RRBS) (Meissner et al., 2005), ATAC-Me is agnostic to

sequence context, thereby yielding better coverage of CpG sites in relevant GREs (namely enhancer regions with lower CpG densities). Additionally, requisite sequencing depths are equivalent to those of standard ATAC-seq, making ATAC-Me a cost-effective way to examine methylation of accessible DNA. As expected, the sequence complexity (or number of distinct reads) in ATAC-Me libraries is lower compared with standard ATAC-seq yet substantially higher than the complexity of ERRBS libraries sequenced to corresponding read depths (Figure S4B). Sequence and mapping statistics are provided in Table S1.

## Rapid Changes in Chromatin Accessibility Correspond to TF Activity at Putative Monocyte and Macrophage Enhancers

Profiling DNAme in the context of chromatin under dynamic conditions is a cornerstone of our approach; therefore, we applied ATAC-Me to a time course of THP-1 exposure to PMA, which induces terminal monocyte-to-macrophage differentiation. To understand temporal peak behaviors, we employed TCseq, an R package that enables quantitative, differential analysis and clustering of count-based epigenomic and transcriptomic datasets (Wu and Gu, 2019). Within the TCseq framework, we used C-means clustering to identify five specific groups of unique peak regions with different accessibility behaviors across the five-point time course (Figure 2A). These groups display distinct behaviors from one another, where peak amplitudes reflect (1) gradual closing response, (2) transient response, (3) early persistent response, (4) gradual opening response, and (5) late response of ChrAcc peak regions (Figures 2B and 2C). Interestingly, only ~12,000 of 90,000 unique peak regions demonstrated dynamic temporal behavior, the majority of which are intergenic or intronic and significantly depleted in promoter proximal regions (Figure S4C).

To assess the probability that similar clustering patterns are produced by random chance from our data, read counts were scrambled between time points and reanalyzed with time structure removed (Figure S5A). C-means maximal probabilities for clusters obtained from scrambled data were much lower than for non-scrambled data (Figure S5B), indicating the temporal specificity of our differential peak calls. We next examined if the temporal trends of different ChrAcc clusters determined entirely with ATAC-Me data would hold true if we substitute key time points (0 and 24 h) with standard ATAC-seq data. Temporal trends among clusters remained strikingly similar even when recalculated with standard ATAC substitute data, again supporting the concordance of ATAC-Me with standard ATAC for profiling ChrAcc dynamics (Figures S5C and S5D).

Significant and differential motif enrichment of specific TFs was observed for each TCseq cluster (Figure 2D). Importantly, high correspondence is observed between cluster-associated TFs and the timeline of early PMA and late PMA response. These TFs include known factors downstream of the protein kinase C pathway, which is a direct target of PMA, and MAPK/ERK signaling (Traore et al., 2005). Within 2 h, accessibility in peak regions enriched for myeloid pioneer factor PU.1(SPI1) and CEBP is significantly reduced, while EGR1 and KLF14 dominate peaks in which accessibility is greatest immediately following PMA addition. NFkB, an important TF in macrophage differentiation and known target of immune regulation genes (Takashiba et al., 1999), emerges as the dominant TF motif within peak regions clustering at 24 h. Methods of identifying TF footprints from DHS and ATAC-seq data have been described (Baek et al., 2017; Piper et al., 2013); thus, we asked whether these patterns are preserved in ATAC-Me data. Despite bisulfite conversion-induced DNA damage, abundant TF footprints are detected (Figure S6A). Accordingly, these footprints are consistent with time point-specific TF binding events, and differential analysis of TF footprints also reveals time point-linked enrichment and depletion of specific TFs (Figure S6B). To provide further support to these observations, we analyzed existing THP-1 monocyte and macrophage chromatin immunoprecipitation sequencing (ChIP-seq) data for acetylated histone H3 lysine 27 (H3K27ac), a mark associated with active enhancers (Figure S7A; Phanstiel et al., 2017). An increase or decrease in H3K27ac can be observed between opening and closing ChrAcc loci, respectively, when comparing unstimulated monocytes with macrophages exposed to PMA for 72 h. This is in contrast to static regions, which overall show very little change in H3K27ac signal. Altogether, these data support that dynamic ChrAcc loci represent activating and responding enhancer elements.

## Transitioning Chromatin Regions Exhibit Prolonged Methylation States at Early Time Points

The identification of highly dynamic ChrAcc loci consisting of newly accessible DNA is advantageous in determining whether the establishment of ChrAcc and loss of DNAme, or vice versa, are distinct events in the ordered process of enhancer regulation, while also capturing the temporal diversity of states that may exist genome-wide. Importantly, we did observe a significant number of accessible regions that were also highly methylated (>50% methylation), which supports our previous observation that "dichotomous" states do exist (Figures 3A and 3B). Comparing methylation levels within dynamic ChrAcc peaks (identified by TCseq) with static peaks, a greater number of hypermethylated regions are observed (Figures 3A and 3B). In other words, if all ChrAcc regions are considered, regardless of whether they change over time, the distribution of methylation is heavily biased toward hypomethylation. However, when we consider only dynamic regions, a substantial number of peaks are hypermethylated, and this hypermethylation persists over time despite increasing levels of accessibility (Figures 3A and 3B). This persistent hypermethylation frequently occurs at "nascent" GREs where little to no accessibility exists prior to PMA treatment (Figure 3B). Likewise, a subset of dynamic ATAC-Me peaks exhibits persistent hypomethylation despite increasing or decreasing peak signals. This phenomenon is more frequent among loci in which low levels of accessibility pre-exist, often corresponding to promoters and other high-density CGI regions, as exemplified by the "transient response" cluster, which is enriched for regions that contain higher CpG densities including promoters (Figures 3B and 3C; Figure S4C). Additionally, the "gradual closing response" peaks also feature persistent hypomethylation despite decreasing levels of accessibility. Although the sampling nature of ATAC-Me can yield sparse read count data at early stages of chromatin opening or late stages of chromatin closing, endpoint-matched WGBS

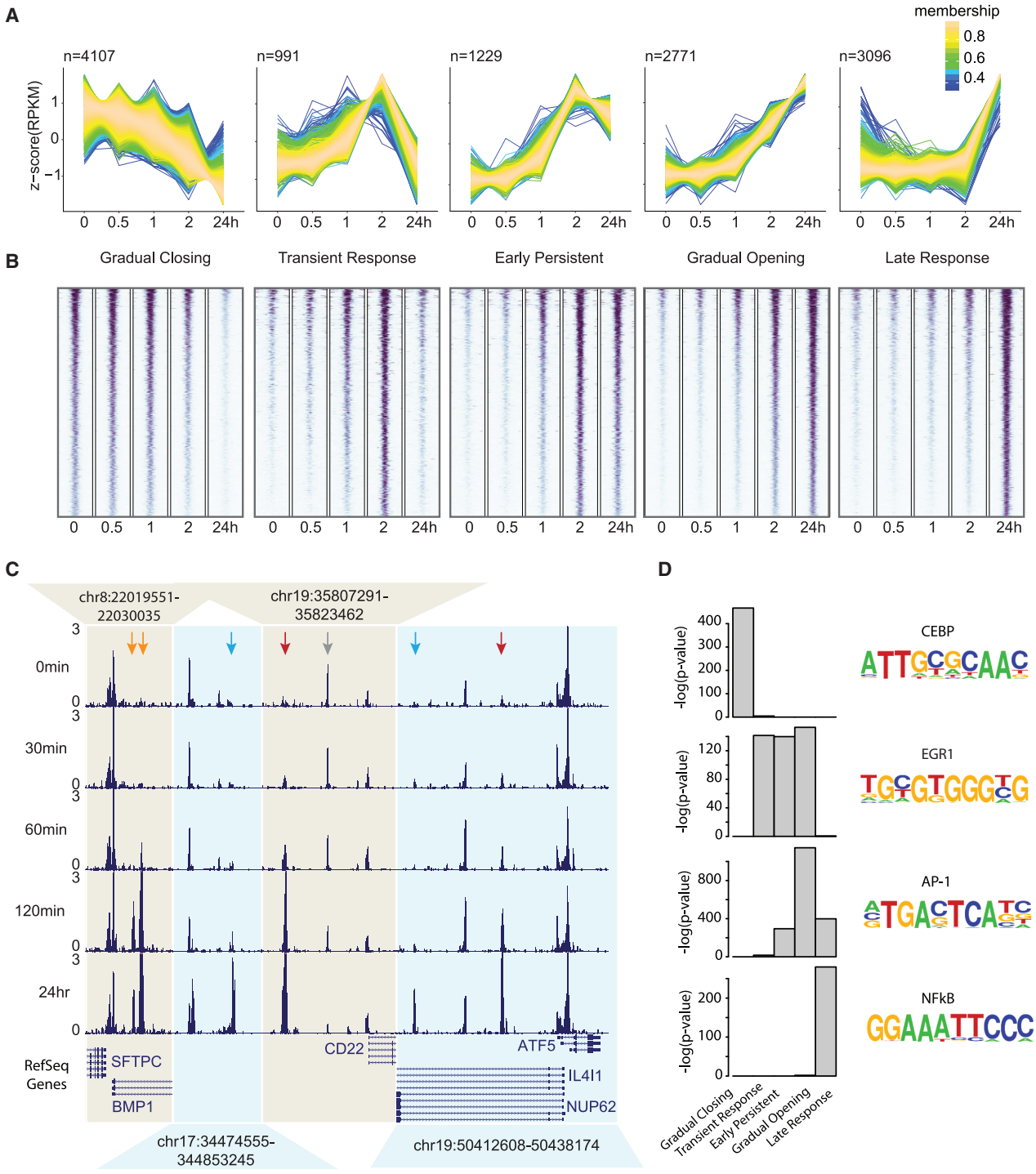


**Figure 2. Dynamic Chromatin Accessibility and Transcription Factor Motif Enrichment during PMA-Stimulated Gene Activation**

(A) C-means clustering of ATAC-Me time course accessibility data reveals multiple categorizations of dynamic accessibility behavior. Membership indicates the goodness of fit for a region in a particular cluster.

(B) Heatmap of ATAC-Me accessibility signal at each time point for the dynamically accessible regions identified with corresponding C-means clustering.

(C) UCSC Genome Browser non-contiguous, "multi-region" view of multiple dynamic loci across time. Colored arrows indicate dynamic peak behaviors: early persistent response (yellow), late response (blue), gradual opening response (red), gradual closing response (gray).

(D) Significance scores (p values) for select transcription factor motif enrichment within accessibility clusters. Motif enrichment p values were calculated using HOMER. Sequence logos for enriched motifs are depicted to the right of motif enrichment plots.

See also Figures S4–S7.

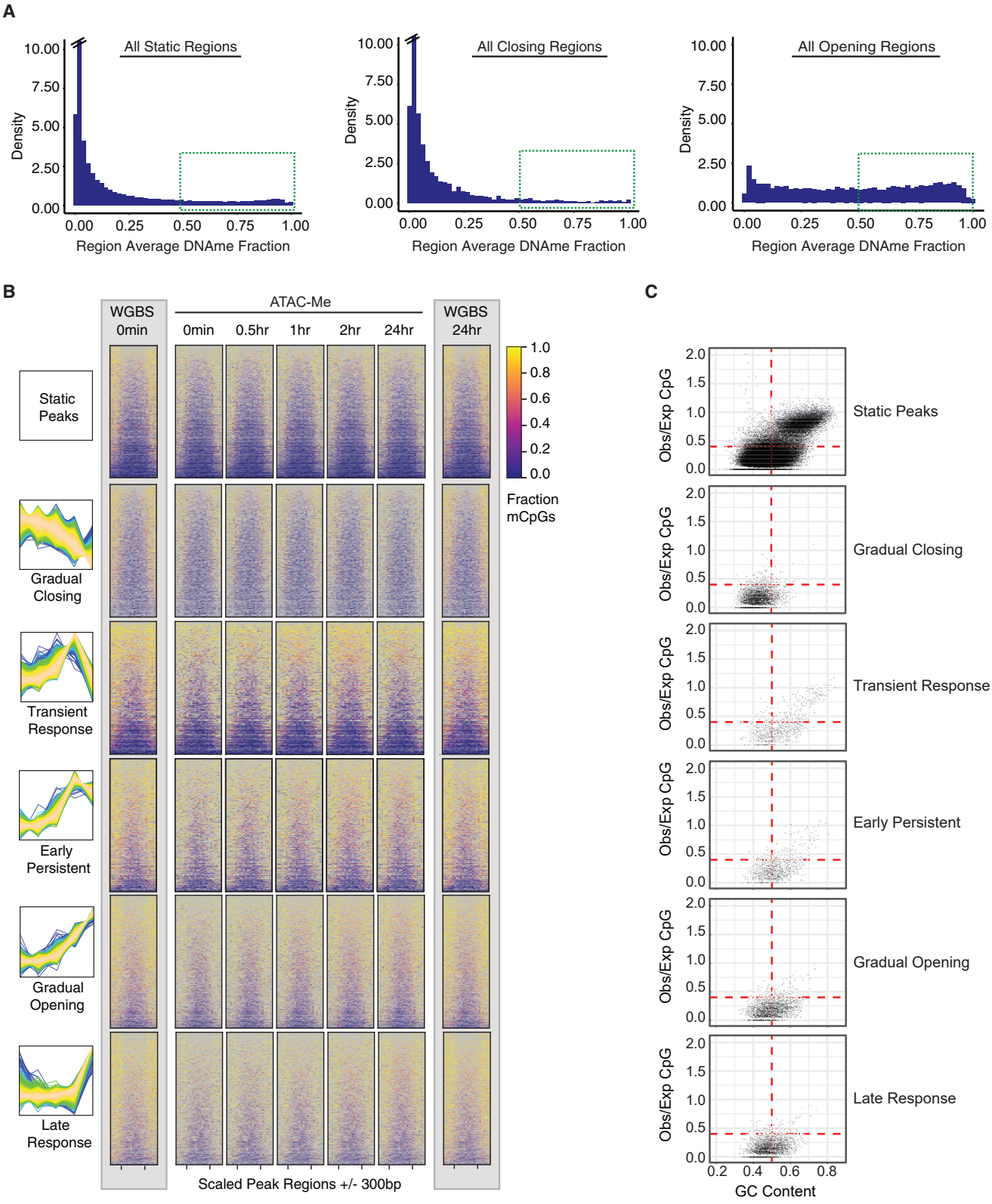


*(legend on next page)*

reference data support these results (Figure 3B). These data suggest that DNAme and ChrAcc dynamics may be quantitatively decoupled and that, although the two states are highly correlated, their spatiotemporal partnership is much less interdependent than previously appreciated.

Previous studies have established that regions with high CpG density are less dynamic and more hypomethylated than regions with lower CpG density. In our data, we detect notable differences in CpG content between clusters of peaks with different temporal ChrAcc behaviors and TF motif enrichments (Figures 2D and 3C). Moreover, the two peak clusters, "transient response" and "early persistent response," that rapidly gain accessibility upon PMA stimulation have the highest CpG content, whereas the more gradual, late responders feature significantly lower frequencies of CpGs. The "transient response" cluster also contains the majority of regions where gains in ChrAcc are characterized by pre-established and consistent hypomethylation. This may be important considering the necessity to invoke rapid control of gene expression without barriers that require additional enzymatic steps and/or DNA replication.

## Transcriptional Responses Track Closely with Chromatin Accessibility

Pathway enrichment analysis of genes in proximity to dynamic ATAC-Me peaks revealed gene sets with distinct functional associations consistent with PMA stimulation of THP-1 cells (Figure 4A). To probe transcriptional changes corresponding to ATAC-Me dynamics, we performed RNA-seq in parallel for each time point collected. Independent K-means clustering of RNA-seq data for the top 20% most variable genes across the time course demonstrates near identical group transcriptional responses to those temporal behaviors exhibited by clusters defined by accessibility (Figure 4B). Importantly, these changes are detected as soon as 0.5 h post-induction and include transcripts of TFs corresponding to TF motifs implicated among the divergent accessibility groups (Figure 4C). Analysis of genes nearest to dynamic ATAC-Me peaks suggests that ChrAcc is a better predictor of transcriptional response than DNAme levels (Figure 4D). Moreover, these dynamic transcriptional responses occur despite persistent DNAme levels of paired peak regions. It is also worth noting that the directionality of change (i.e., accessibility and transcription) is not always uniform, as exemplified by gene pairs of "gradually closing" peaks that display increases in transcription. This may be explained by (1) inaccurate assignment of biological gene:peak pairs or (2) the possibility of the GRE's being either an enhancer or a repressor. It is also important to note that although DNAme levels are less dynamic over time, gene-associated peak regions consist of a range of methylation values (Figure 4D).

To further investigate these relationships, we globally compared transcript abundances with either accessibility or DNAme levels for the top 20% most variable genes paired with nearest neighbor peaks, finding a stronger positive correlation with accessibility compared with a weaker negative correlation with DNAme (Figure 5A). We considered that because of the distinct characteristics of each data type, data standardization is required to describe the temporal relationships among these three molecular events. Therefore, a standardized difference from the mean across all time points was determined for every dynamic peak:gene pair (Figures 5B and 6D). This analysis revealed a tight temporal relationship between ChrAcc and transcriptional dynamics, but not DNAme. Related to these observations, a significant feature of the THP-1 monocyte-to-macrophage system is that replicative potential is irreversibly lost upon PMA exposure, and replication may be required for both deposition and removal of DNAme (Figure S7B) (Donaghey et al., 2018; Otani et al., 2013). Nonetheless, our data suggest that gain or loss of DNAme is not immediately required for gene or GRE activation (or repression) to occur.

## Subtle Loss of DNAme Occurs Downstream of Chromatin and Transcriptional Changes

Thus far our analyses have focused on a relatively short-term time course of PMA induction. Within this short time frame, DNAme states do not appear to change among regions undergoing rapid ChrAcc changes. These results suggest that ChrAcc and DNAme changes do not occur on the same timescale, raising the possibility that DNAme changes occur as a secondary response to ChrAcc changes. Focusing specifically on ChrAcc regions that open by 24 h (~7,000 loci), we performed an extended time course of PMA induction, collecting ATAC-Me data at 0, 24, 48, and 72 h. For ChrAcc regions that begin to open by 24 h, accessibility has largely plateaued by 48 and 72 h (Figure 6A). Surprisingly, some small but significant loss of DNAme is observed within these regions by 72 h (Figures 6B–6D), further highlighting a molecular decoupling of ChrAcc and DNAme programs.

Several recent lines of evidence support these data (discussed in further detail below); nonetheless, we sought to verify the competence of ATAC-Me to capture distinct changes in DNAme. At an applied concentration of 350 μM, vitamin C has been demonstrated to induce "artificial" hypomethylation of select genomic regions by enhancing the catalytic activity of TET-family DNA dioxygenases involved in DNA demethylation pathways

**Figure 3. Genomic Regions with Rapid Chromatin Accessibility Dynamics Exhibit Prolonged Methylation**

(A) Density histogram of average methylation fraction for static accessible regions (no membership to a TCseq cluster) across the time course, regions with decreasing accessibility signal across time (gradual closing response), and regions with increasing accessibility signal (late + gradual opening + transient + early persistent responses identified with TCseq). Green boxes highlight regions with >50% DNA methylation.

(B) Heatmaps display mCpG fraction across individual peak regions in different accessibility groups (static, gradual closing response, transient response, early persistent response, gradual opening response, and late response). mCpG fraction is calculated in 50 bp bins across regions scaled to 600 bp with a flanking region of ±300 bp.

(C) CpG density and GC content of TCseq cluster regions dynamic for chromatin accessibility across time. CpG density was calculated as observed/expected occurrence of CpG dinucleotides within TCseq cluster regions defined in Figure 2. Dashed lines represent CpG island thresholds defined by Gardiner-Garden and Frommer (1987) for CpG density/GC content.

See also Figure S7.

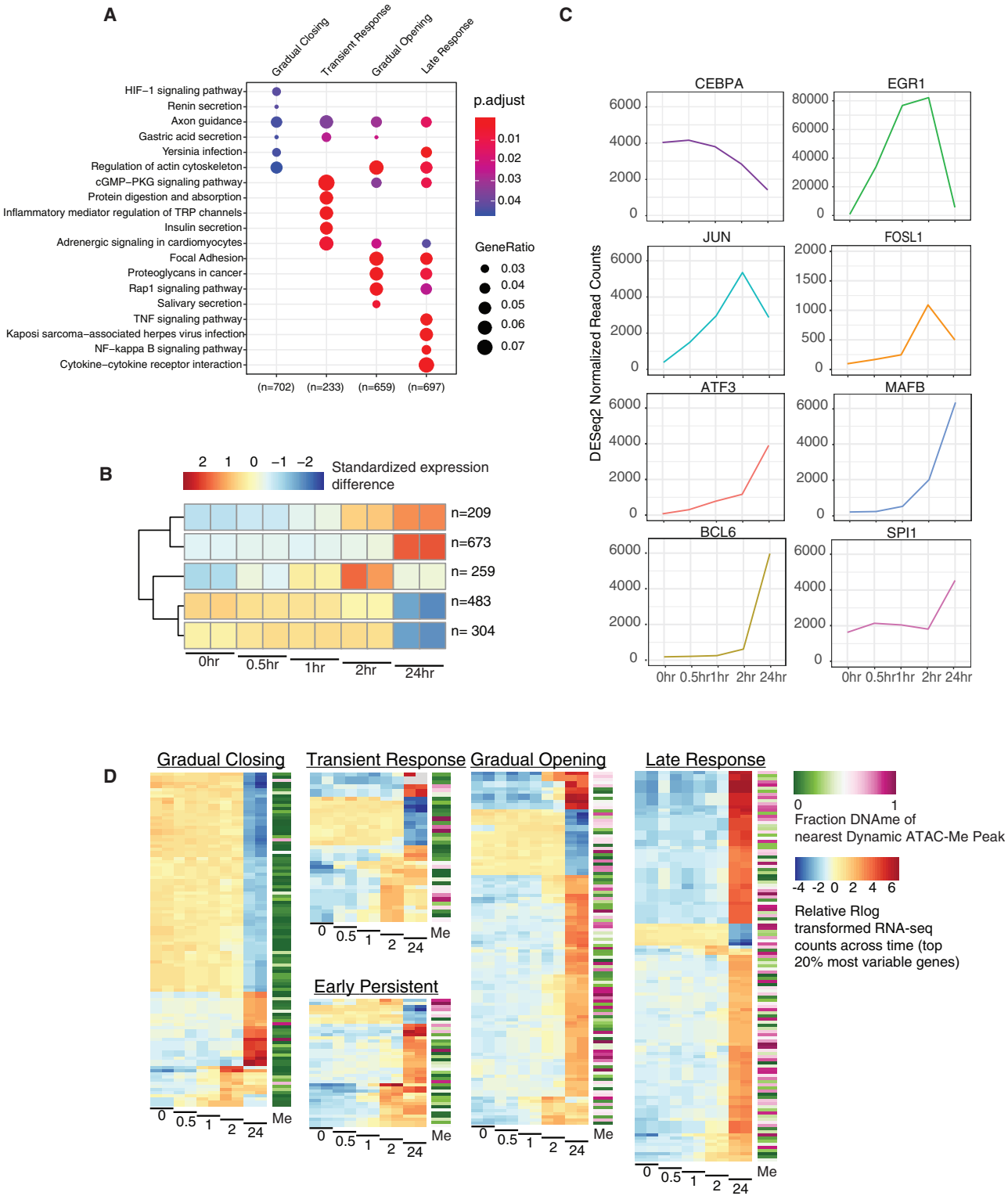


**Figure 4. Transcriptional Changes Track with Chromatin Accessibility Behaviors Independently of Methylation**

(A) KEGG pathway enrichment of genes proximal to dynamic peaks in specific TC-seq clusters.

(B) K-means clustering of the top 20% most variable genes identified with RNA-seq.

(C) Read count plots across time for select TFs known to be related to the monocyte-to-macrophage transition. Depicted values are a replicate average of DESeq2 normalized read counts.

*(legend continued on next page)*

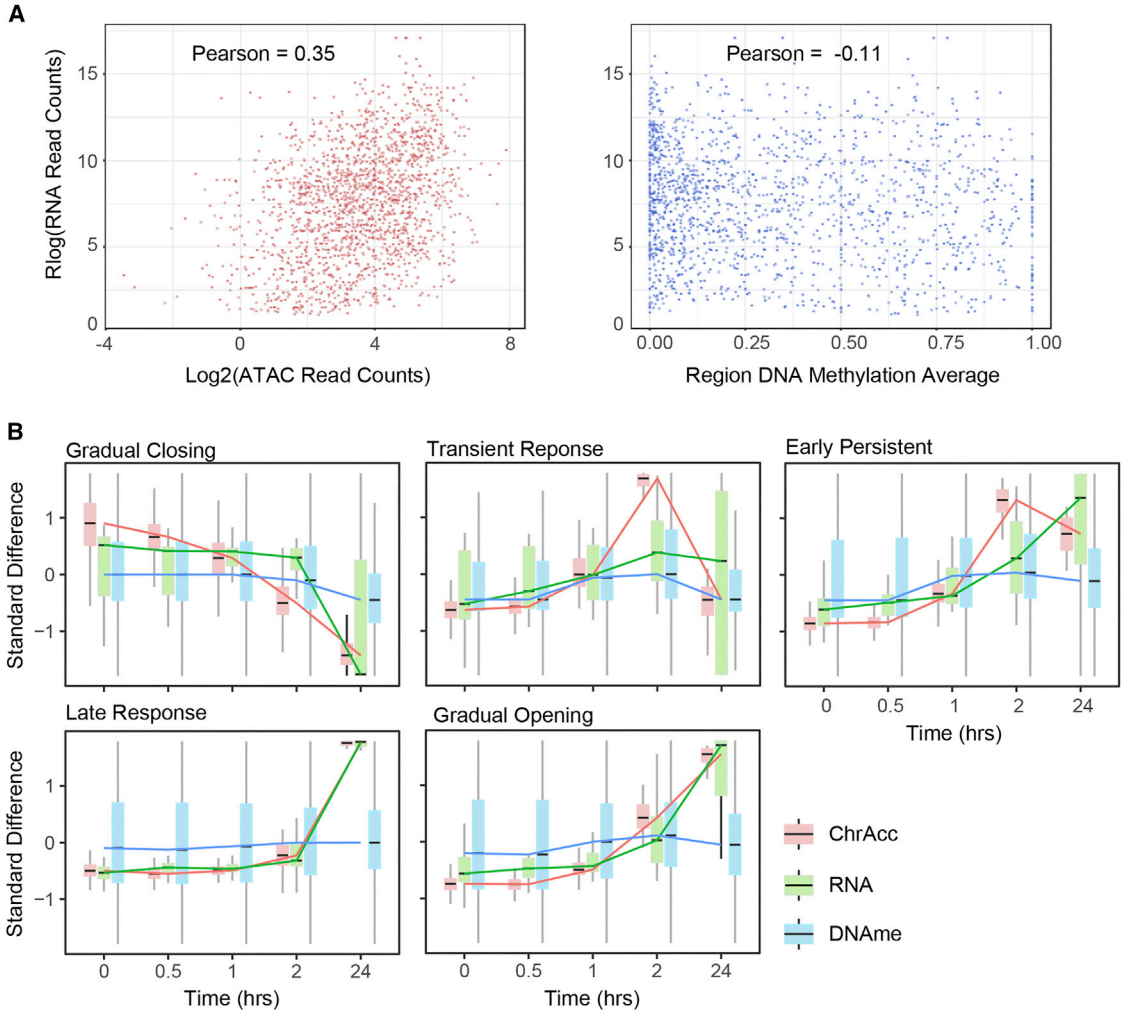


**Figure 5. Integrating the Dynamics of Chromatin Accessibility, DNA Methylation, and Transcription**

(A) Scatterplot of RNA-seq read abundance for the top 20% most variable genes associated with a dynamic chromatin-accessible locus plotted against neighboring dynamic chromatin-accessible locus read counts (left; Pearson $r = 0.35$, $p < 0.0001$) or average CpG DNA methylation (right; Pearson $r = -0.11$, $p < 0.0001$). Scatterplots represent all time points (0, 0.5, 1, 2, and 24 h) plotted simultaneously.

(B) Boxplot distributions of standardized difference across time for all dynamic loci defined by TC-seq. Standardized difference across time was calculated for normalized ATAC read counts, rlog(read counts) of neighboring transcripts (top 20% most variable), and the DNA methylation state of the chromatin-accessible DNA fragments. Lines represent median values.

(Blaschke et al., 2013; Cimmino et al., 2017). In conjunction with PMA induction, we added stabilized vitamin C (L-AA-2-P) to THP-1 cells for a course of 72 h. At the aforementioned "opening" regions, we observe significant reduction in DNAme in the presence of vitamin C compared with control conditions (PMA alone; Figures 6B–6D). Therefore, loss of DNAme is observed only after application of a considerable stimulus of a DNA demethylation pathway. Overall, these data confirm both the biological coincidence of DNAme within ChrAcc regions and a spatiotemporal disconnect between DNAme and ChrAcc dynamics at enhancers during terminal cell fate transitions.

## DISCUSSION

Many aspects of gene regulation are deeply conserved in eukaryotes and have been extensively studied in model organisms, but DNAme and its relationship with other critical aspects of enhancer regulation are not well understood. Genes are activated sequentially, and according to current models, enhancer chromatin states are modified by a series of biochemical events, including pioneer factor-initiated recruitment of chromatin remodelers and histone modifiers, leading to the appearance of chromatin-accessible DNA sites

(D) Hierarchical clustering of the top 20% most variable genes in nearby proximity to genomic loci identified as dynamic for chromatin accessibility. The mean mCpG fraction of all time points for neighboring ATAC-Me peaks is indicated to the right of each plot. Black bars below the plots indicate replicate pairs for each time point.

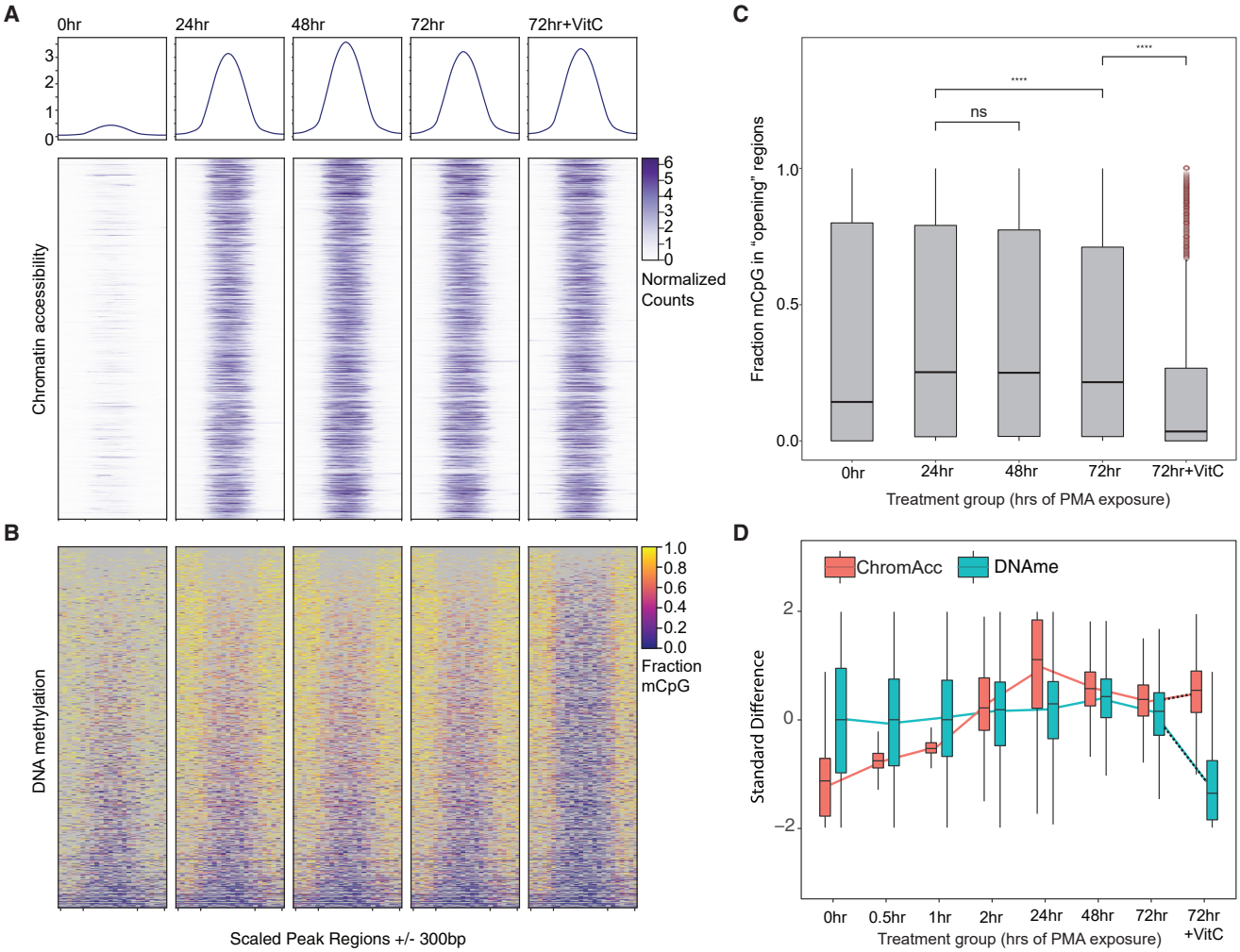


**Figure 6. Loss of DNA Methylation Is Delayed in Nascent Open Chromatin Regions**

(A) Heatmap of ATAC-Me accessibility signal for extended time points across all genomic loci exhibiting accessibility by 24 h (early persistent response + gradual opening response + late response).

(B) Heatmaps display CpG methylation levels in 50 bp bins across all regions in (A).

(C) Boxplot distribution comparisons of methylated CpG fractions across extended time points and treatments. Wilcoxon rank-sum test was used for statistical comparison (ns, not significant). Red points indicate outlier values.

(D) Boxplot distributions of standardized difference across early and late time points for all genomic regions opening at 24 h (A and B). Standardized difference across time was calculated for normalized ATAC read counts and CpG methylation fraction within chromatin-accessible fragments. Lines represent median values.

See also Figure S7.

(Levine et al., 2014). DNAme is not typically permissive to transcription (Schübeler, 2015; Stein et al., 1982; Vardimon et al., 1982), and transcription at enhancers can be detected prior to promoter activation (Arner et al., 2015). So, loss of DNAme, whether immediate or eventual, is also expected at these sites. A variety of indirect evidence points to active removal of DNAme, including the presence of hydroxymethylation (5hmC) at cell fate-determining enhancers (Li et al., 2018a; Sérandour et al., 2012) and recruitment of TET enzymes by pioneer factors (Li et al., 2018b; Lio et al., 2016). Furthermore, we and others have shown that enhancer hypomethylation is highly cell type specific and a better predictor of target gene transcription than promoter hypomethylation (Schlesinger et al., 2013). In light of these ideas, a key premise for performing ATAC-Me stemmed from the observation that an unexpected fraction of DHS sites ascertained by DHS-seq are methylated in WGBS datasets of the equivalent cell type, a duality we reasoned may represent an intermediate state along a continuum of enhancer activation. Other studies support these observations, reporting "bivalent" regions of H3K27ac being marked by DNAme (Charlet et al., 2016). Accordingly, time is an equally vital component to our approach, as we sought to capture both ChrAcc and DNAme changes during cell fate transitions.

ATAC-Me is a straightforward approach that detects DNAme of accessible DNA fragments from native chromatin and requires minimal molecular adaptation of existing Tn5-assisted methods including ATAC-seq and tagmentation-based WGBS. ATAC-Me allows quantification of accumulating DNA fragments in accessible genomic regions (or in nascent opening regions); therefore, direct interrogation of the temporal relationship between ChrAcc and DNAme is possible in a rapidly changing chromatin environment. Additionally, ATAC-Me provides a focused view of the methylome most relevant to cellular function; the methylome of DNA molecules accessible to enzymes and TFs facilitating gene regulation. Although approaches that enable joint profiling of chromatin features and DNAme, including NOME-seq (nucleosome occupancy and methylome sequencing), scNMT-seq (single-cell nucleosome, methylation, and transcription sequencing), and ChIP-BS (ChIP coupled with bisulfite sequencing) have been described, ATAC-Me offers some key advantages (Brinkman et al., 2012; Clark et al., 2018; Kelly et al., 2012). First, ATAC-Me is not limited by cytosine frequency in specific dinucleotide contexts, so even the most CpG-poor enhancers are evaluated. Notably, our method is readily able to identify TF footprints, and the DNAme state of putative TF footprint sites can be calculated, a feature that distinguishes ATAC-Me from other approaches. Second, ATAC-Me selectively enriches Tn5-accessible genomic regions, so fewer sequence reads (50 million to 60 million) are necessary to obtain high, focused coverage of accessible DNA, compared with whole-genome approaches. Use of a transposome assembly (Picelli et al., 2014) with methylated adaptors also allows direct cloning of accessible fragments with minimal opportunities for input loss and therefore many fewer cells (50,000–200,000) are required compared with other methods.

Using ATAC-Me, we observe clear patterns of rapid ChrAcc that are tightly associated with the time points measured. Although this time course sampled both very early (0, 0.5, 1, and 2 h) and later (24, 48, and 72 h) time points, our results indicate that ChrAcc dynamics responses seem to plateau by 24 h. It remains to be seen if additional waves of ChrAcc are observed at time points beyond 72 h (for example with stimulation of different activation states of macrophages). ATAC-Me detected TF footprints and distinct pattern-specific TF motifs that tracked closely with time, even for time points separated by less than 2 h, reflecting the rapid responses of ChrAcc within this time frame. Transcriptional changes also follow similar patterns to those observed with accessibility. In contrast, we observe a range of DNAme states associated with accessibility changes. Importantly, DNAme showed only minimal changes within this time frame in our THP-1 monocyte-to-macrophage model. This surprising temporal disconnect between DNAme, ChrAcc, and transcription suggests that loss of DNAme is not immediately required for transcription or for TF binding, an observation supported by several lines of evidence. In particular, a recent study showed that DNA demethylation is not required for pioneer FoxA2 occupancy and its concomitant effects on ChrAcc (Donaghey et al., 2018). Moreover, in dendritic cells, gene upregulation is observed ahead of DNAme changes in response to bacterial infection (Pacis et al., 2015).

Enhancer regions that remain methylated despite increasing accessibility may be marked by 5hmC, which would not be distinguished from 5mC in our assay. However, application of high levels of vitamin C induced considerable loss of DNAme by 72 h, indicating that non-physiological levels of vitamin C accelerate methylation removal. These data also imply that the higher levels of DNAme we observe in dynamic ChrAcc peaks is not likely a result of failure to discriminate 5hmC from 5mC. The slight loss of DNAme we observe in the absence of vitamin C suggests that with enough time, the DNAme in these regions will eventually be lost, though recent evidence suggests that replication is required for extensive DNA demethylation (Barwick et al., 2016; Donaghey et al., 2018; Otani et al., 2013). THP-1 macrophages, like dendritic cells, are terminally differentiated and no longer replicate. Indeed, the question remains if DNAme would be more dynamic in a cell fate specification system that maintains cell division status. Nevertheless, our data demonstrate the importance of evaluating DNAme in the context of a changing chromatin environment during cellular differentiation. ATAC-Me may also provide the resolution to catalog precise epigenetic events that lead to sequential cell fate decisions in normal and abnormal cell fate models.

## Limitations

Some noteworthy limitations of ATAC-Me are that the approach relies on the assumption that inaccessible loci, and therefore missing data, are methylated, so a complementary WGBS dataset may be useful in some cases. ATAC-inspired methodologies are also plagued by mitochondrial DNA contamination, which can be minimized by use of modified lysis protocols (Corces et al., 2017) that include digitonin or depletion by Cas9 paired with a library of mitochondrial guide RNAs (Montefiori et al., 2017).

## STAR★METHODS

Detailed methods are provided in the online version of this paper and include the following:

- KEY RESOURCES TABLE
- LEAD CONTACT AND MATERIALS AVAILABILITY
- EXPERIMENTAL MODEL AND SUBJECT DETAILS
  - THP-1 monocytes
  - *Drosophila* S2 Cells
- METHOD DETAILS
  - Cell Treatments
  - Transposome Preparation
  - ATAC-seq
  - ATAC-Me
  - THP-1 T-WGBS
  - *Drosophila* S2 cell T-WGBS
  - RNA-seq
  - Sequencing Library Processing
- QUANTIFICATION AND STATISTICAL ANALYSIS
- DATA AND CODE AVAILABILITY
- ADDITIONAL RESOURCES

### SUPPLEMENTAL INFORMATION

Supplemental Information can be found online at https://doi.org/10.1016/j.molcel.2020.01.004.

## ACKNOWLEDGMENTS

We thank M. Ascano, T. Capra, D. Cortez, S. Hiebert, and our peer reviewers for helpful comments in preparing this manuscript. We thank Lindsey Guerin for her input in ChIP-seq analysis and graphical abstract artwork. We also thank R. Sanberg for kindly providing the Tn5 plasmid and purification protocols. We are grateful for support of the project and the time invested in producing this manuscript by the National Institutes of Health (K22 CA184308 to E.H., T32HD007502 to K.R.B., and NIH R01 HG007650 to A.D.S.).

## AUTHOR CONTRIBUTIONS

Conceptualization, E.H. and K.R.B.; Methodology, E.H. and K.R.B.; Investigation, K.R.B., T.J.H., J.A., and B.C.; Formal Analysis, K.R.B., B.E.D., T.J.S., and A.D.S.; Writing – Original Draft, E.H. and K.R.B.; Writing – Review & Editing, E.H., K.R.B., B.E.D., and A.D.S.; Funding Acquisition, E.H. and A.D.S.; Resources, E.H. and K.R.B.; Supervision, E.H. and A.D.S.

## DECLARATION OF INTERESTS

The authors declare no competing interests.

Received: March 6, 2019
Revised: November 8, 2019
Accepted: January 2, 2020
Published: January 29, 2020

## REFERENCES

Adey, A., and Shendure, J. (2012). Ultra-low-input, tagmentation-based whole-genome bisulfite sequencing. Genome Res. *22*, 1139–1143.

Akalin, A., Garrett-Bakelman, F.E., Kormaksson, M., Busuttil, J., Zhang, L., Khrebtukova, I., Milne, T.A., Huang, Y., Biswas, D., Hess, J.L., et al. (2012). Base-pair resolution DNA methylation sequencing reveals profoundly divergent epigenetic landscapes in acute myeloid leukemia. PLoS Genet. *8*, e1002781.

Arner, E., Daub, C.O., Vitting-Seerup, K., Andersson, R., Lilje, B., Drabløs, F., Lennartsson, A., Rönnerblad, M., Hrydziuszko, O., Vitezic, M., et al.; FANTOM Consortium (2015). Transcribed enhancers lead waves of coordinated transcription in transitioning mammalian cells. Science *347*, 1010–1014.

Baek, S., Goldstein, I., and Hager, G.L. (2017). Bivariate genomic footprinting detects changes in transcription factor activity. Cell Rep. *19*, 1710–1722.

Barwick, B.G., Scharer, C.D., Bally, A.P.R., and Boss, J.M. (2016). Plasma cell differentiation is coupled to division-dependent DNA hypomethylation and gene regulation. Nat. Immunol. *17*, 1216–1225.

Blaschke, K., Ebata, K.T., Karimi, M.M., Zepeda-Martínez, J.A., Goyal, P., Mahapatra, S., Tam, A., Laird, D.J., Hirst, M., Rao, A., et al. (2013). Vitamin C induces Tet-dependent DNA demethylation and a blastocyst-like state in ES cells. Nature *500*, 222–226.

Bock, C., Beerman, I., Lien, W.H., Smith, Z.D., Gu, H., Boyle, P., Gnirke, A., Fuchs, E., Rossi, D.J., and Meissner, A. (2012). DNA methylation dynamics during in vivo differentiation of blood and skin stem cells. Mol. Cell *47*, 633–647.

Brinkman, A.B., Gu, H., Bartels, S.J., Zhang, Y., Matarese, F., Simmer, F., Marks, H., Bock, C., Gnirke, A., Meissner, A., and Stunnenberg, H.G. (2012). Sequential ChIP-bisulfite sequencing enables direct genome-scale investigation of chromatin and DNA methylation cross-talk. Genome Res. *22*, 1128–1138.

Buenrostro, J.D., Giresi, P.G., Zaba, L.C., Chang, H.Y., and Greenleaf, W.J. (2013). Transposition of native chromatin for fast and sensitive epigenomic profiling of open chromatin, DNA-binding proteins and nucleosome position. Nat. Methods *10*, 1213–1218.

Charlet, J., Duymich, C.E., Lay, F.D., Mundbjerg, K., Dalsgaard Sørensen, K., Liang, G., and Jones, P.A. (2016). Bivalent regions of cytosine methylation and H3K27 acetylation suggest an active role for DNA methylation at enhancers. Mol. Cell *62*, 422–431.

Chen, H., Smith, A.D., and Chen, T. (2016). WALT: fast and accurate read mapping for bisulfite sequencing. Bioinformatics *32*, 3507–3509.

Cimmino, L., Dolgalev, I., Wang, Y., Yoshimi, A., Martin, G.H., Wang, J., Ng, V., Xia, B., Witkowski, M.T., Mitchell-Flack, M., et al. (2017). Restoration of TET2 function blocks aberrant self-renewal and leukemia progression. Cell *170*, 1079–1095.e20.

Clark, S.J., Argelaguet, R., Kapourani, C.A., Stubbs, T.M., Lee, H.J., Alda-Catalinas, C., Krueger, F., Sanguinetti, G., Kelsey, G., Marioni, J.C., et al. (2018). scNMT-seq enables joint profiling of chromatin accessibility DNA methylation and transcription in single cells. Nat. Commun. *9*, 781.

Corces, M.R., Trevino, A.E., Hamilton, E.G., Greenside, P.G., Sinnott-Armstrong, N.A., Vesuna, S., Satpathy, A.T., Rubin, A.J., Montine, K.S., Wu, B., et al. (2017). An improved ATAC-seq protocol reduces background and enables interrogation of frozen tissues. Nat. Methods *14*, 959–962.

Daley, T., and Smith, A.D. (2013). Predicting the molecular complexity of sequencing libraries. Nat. Methods *10*, 325–327.

Dawlaty, M.M., Breiling, A., Le, T., Barrasa, M.I., Raddatz, G., Gao, Q., Powell, B.E., Cheng, A.W., Faull, K.F., Lyko, F., and Jaenisch, R. (2014). Loss of Tet enzymes compromises proper differentiation of embryonic stem cells. Dev. Cell *29*, 102–111.

Dobin, A., Davis, C.A., Schlesinger, F., Drenkow, J., Zaleski, C., Jha, S., Batut, P., Chaisson, M., and Gingeras, T.R. (2013). STAR: ultrafast universal RNA-seq aligner. Bioinformatics *29*, 15–21.

Donaghey, J., Thakurela, S., Charlton, J., Chen, J.S., Smith, Z.D., Gu, H., Pop, R., Clement, K., Stamenova, E.K., Karnik, R., et al. (2018). Genetic determinants and epigenetic effects of pioneer-factor occupancy. Nat. Genet. *50*, 250–258.

Dunwell, T.L., and Pfeifer, G.P. (2014). Drosophila genomic methylation: new evidence and new questions. Epigenomics *6*, 459–461.

Ernst, J., and Kellis, M. (2012). ChromHMM: automating chromatin-state discovery and characterization. Nat. Methods *9*, 215–216.

Fang, F., Hodges, E., Molaro, A., Dean, M., Hannon, G.J., and Smith, A.D. (2012). Genomic landscape of human allele-specific DNA methylation. Proc. Natl. Acad. Sci. U S A *109*, 7332–7337.

Gardiner-Garden, M., and Frommer, M. (1987). CpG islands in vertebrate genomes. J. Mol. Biol. *196*, 261–282.

Hah, N., Danko, C.G., Core, L., Waterfall, J.J., Siepel, A., Lis, J.T., and Kraus, W.L. (2011). A rapid, extensive, and transient transcriptional response to estrogen signaling in breast cancer cells. Cell *145*, 622–634.

Heinz, S., Benner, C., Spann, N., Bertolino, E., Lin, Y.C., Laslo, P., Cheng, J.X., Murre, C., Singh, H., and Glass, C.K. (2010). Simple combinations of lineage-determining transcription factors prime cis-regulatory elements required for macrophage and B cell identities. Mol. Cell *38*, 576–589.

Hodges, E., Molaro, A., Dos Santos, C.O., Thekkat, P., Song, Q., Uren, P.J., Park, J., Butler, J., Rafii, S., McCombie, W.R., et al. (2011). Directional DNA methylation changes and complex intermediate states accompany lineage specificity in the adult hematopoietic compartment. Mol. Cell *44*, 17–28.

Jadhav, U., Cavazza, A., Banerjee, K.K., Xie, H., O'Neill, N.K., Saenz-Vash, V., Herbert, Z., Madha, S., Orkin, S.H., Zhai, H., et al. (2019). Extensive recovery of embryonic enhancer and gene memory stored in hypomethylated enhancer DNA. Mol. Cell *74*, 542–554.e5.

Kelly, T.K., Liu, Y., Lay, F.D., Liang, G., Berman, B.P., and Jones, P.A. (2012). Genome-wide mapping of nucleosome positioning and DNA methylation within individual DNA molecules. Genome Res. *22*, 2497–2506.

Lander, E.S., Linton, L.M., Birren, B., Nusbaum, C., Zody, M.C., Baldwin, J., Devon, K., Dewar, K., Doyle, M., FitzHugh, W., et al.; International Human Genome Sequencing Consortium (2001). Initial sequencing and analysis of the human genome. Nature *409*, 860–921.

Langmead, B., and Salzberg, S.L. (2012). Fast gapped-read alignment with Bowtie 2. Nat. Methods *9*, 357–359.

Levine, M., Cattoglio, C., and Tjian, R. (2014). Looping back to leap forward: transcription enters a new era. Cell *157*, 13–25.

Li, Y., and Tollefsbol, T.O. (2011). Combined chromatin immunoprecipitation and bisulfite methylation sequencing analysis. Methods Mol. Biol. *791*, 239–251.

Li, H., Handsaker, B., Wysoker, A., Fennell, T., Ruan, J., Homer, N., Marth, G., Abecasis, G., and Durbin, R.; 1000 Genome Project Data Processing Subgroup (2009). The Sequence Alignment/Map format and SAMtools. Bioinformatics *25*, 2078–2079.

Li, J., Wu, X., Zhou, Y., Lee, M., Guo, L., Han, W., Mo, W., Cao, W.M., Sun, D., Xie, R., and Huang, Y. (2018a). Decoding the dynamic DNA methylation and hydroxymethylation landscapes in endodermal lineage intermediates during pancreatic differentiation of hESC. Nucleic Acids Res. *46*, 2883–2900.

Li, R., Cauchy, P., Ramamoorthy, S., Boller, S., Chavez, L., and Grosschedl, R. (2018b). Dynamic EBF1 occupancy directs sequential epigenetic and transcriptional events in B-cell programming. Genes Dev. *32*, 96–111.

Lio, C.W., Zhang, J., González-Avalos, E., Hogan, P.G., Chang, X., and Rao, A. (2016). Tet2 and Tet3 cooperate with B-lineage transcription factors to regulate DNA modification and chromatin accessibility. eLife *5*, e18290.

Lister, R., Pelizzola, M., Dowen, R.H., Hawkins, R.D., Hon, G., Tonti-Filippini, J., Nery, J.R., Lee, L., Ye, Z., Ngo, Q.M., et al. (2009). Human DNA methylomes at base resolution show widespread epigenomic differences. Nature *462*, 315–322.

Love, M.I., Huber, W., and Anders, S. (2014). Moderated estimation of fold change and dispersion for RNA-seq data with DESeq2. Genome Biol. *15*, 550.

Lu, H., Yuan, Z., Tan, T., Wang, J., Zhang, J., Luo, H.J., Xia, Y., Ji, W., and Gao, F. (2015). Improved tagmentation-based whole-genome bisulfite sequencing for input DNA from less than 100 mammalian cells. Epigenomics *7*, 47–56.

Martin, M. (2011). Cutadapt removes adapter sequences from high-throughput sequencing reads. EMBnet.journal *17*, 12.

Martos, S.N., Li, T., Ramos, R.B., Lou, D., Dai, H., Xu, J.C., Gao, G., Gao, Y., Wang, Q., An, C., et al. (2017). Two approaches reveal a new paradigm of 'switchable or genetics-influenced allele-specific DNA methylation' with potential in human disease. Cell Discov. *3*, 17038.

Mayran, A., Khetchoumian, K., Hariri, F., Pastinen, T., Gauthier, Y., Balsalobre, A., and Drouin, J. (2018). Pioneer factor Pax7 deploys a stable enhancer repertoire for specification of cell fate. Nat. Genet. *50*, 259–269.

Meissner, A., Gnirke, A., Bell, G.W., Ramsahoye, B., Lander, E.S., and Jaenisch, R. (2005). Reduced representation bisulfite sequencing for comparative high-resolution DNA methylation analysis. Nucleic Acids Res. *33*, 5868–5877.

Montefiori, L., Hernandez, L., Zhang, Z., Gilad, Y., Ober, C., Crawford, G., Nobrega, M., and Jo Sakabe, N. (2017). Reducing mitochondrial reads in ATAC-seq using CRISPR/Cas9. Sci. Rep. *7*, 2451.

Okano, M., Bell, D.W., Haber, D.A., and Li, E. (1999). DNA methyltransferases Dnmt3a and Dnmt3b are essential for de novo methylation and mammalian development. Cell *99*, 247–257.

Otani, J., Kimura, H., Sharif, J., Endo, T.A., Mishima, Y., Kawakami, T., Koseki, H., Shirakawa, M., Suetake, I., and Tajima, S. (2013). Cell cycle-dependent turnover of 5-hydroxymethyl cytosine in mouse embryonic stem cells. PLoS ONE *8*, e82961.

Pacis, A., Tailleux, L., Morin, A.M., Lambourne, J., MacIsaac, J.L., Yotova, V., Dumaine, A., Danckaert, A., Luca, F., Grenier, J.C., et al. (2015). Bacterial infection remodels the DNA methylation landscape of human dendritic cells. Genome Res. *25*, 1801–1811.

Phanstiel, D.H., Van Bortle, K., Spacek, D., Hess, G.T., Shamim, M.S., Machol, I., Love, M.I., Aiden, E.L., Bassik, M.C., and Snyder, M.P. (2017). Static and dynamic DNA loops form AP-1-bound activation hubs during macrophage development. Mol. Cell *67*, 1037–1048.e6.

Picelli, S., Björklund, A.K., Reinius, B., Sagasser, S., Winberg, G., and Sandberg, R. (2014). Tn5 transposase and tagmentation procedures for massively scaled sequencing projects. Genome Res. *24*, 2033–2040.

Piper, J., Elze, M.C., Cauchy, P., Cockerill, P.N., Bonifer, C., and Ott, S. (2013). Wellington: a novel method for the accurate identification of digital genomic footprints from DNase-seq data. Nucleic Acids Res. *41*, e201.

Quinlan, A.R., and Hall, I.M. (2010). BEDTools: a flexible suite of utilities for comparing genomic features. Bioinformatics *26*, 841–842.

Rada-Iglesias, A., Bajpai, R., Prescott, S., Brugmann, S.A., Swigut, T., and Wysocka, J. (2012). Epigenomic annotation of enhancers predicts transcriptional regulators of human neural crest. Cell Stem Cell *11*, 633–648.

Ramírez, F., Dündar, F., Diehl, S., Grüning, B.A., and Manke, T. (2014). deepTools: a flexible platform for exploring deep-sequencing data. Nucleic Acids Res. *42*, W187–W191.

Schlesinger, F., Smith, A.D., Gingeras, T.R., Hannon, G.J., and Hodges, E. (2013). De novo DNA demethylation and noncoding transcription define active intergenic regulatory elements. Genome Res. *23*, 1601–1614.

Schübeler, D. (2015). Function and information content of DNA methylation. Nature *517*, 321–326.

Sérandour, A.A., Avner, S., Oger, F., Bizot, M., Percevault, F., Lucchetti-Miganeh, C., Palierne, G., Gheeraert, C., Barloy-Hubler, F., Péron, C.L., et al. (2012). Dynamic hydroxymethylation of deoxyribonucleic acid marks differentiation-associated enhancers. Nucleic Acids Res. *40*, 8255–8265.

Shibata, H., Yoshino, K., Sunahara, S., Gondo, Y., Katsuki, M., Ueda, T., Kamiya, M., Muramatsu, M., Murakami, Y., Kalcheva, I., et al. (1996). Inactive allele-specific methylation and chromatin structure of the imprinted gene U2af1-rs1 on mouse chromosome 11. Genomics *35*, 248–252.

Song, Q., Decato, B., Hong, E.E., Zhou, M., Fang, F., Qu, J., Garvin, T., Kessler, M., Zhou, J., and Smith, A.D. (2013). A reference methylome database and analysis pipeline to facilitate integrative and comparative epigenomics. PLoS ONE *8*, e81148.

Spektor, R., Tippens, N.D., Mimoso, C.A., and Soloway, P.D. (2019). methyl-ATAC-seq measures DNA methylation at accessible chromatin. Genome Res. *29*, 969–977.

Stadler, M.B., Murr, R., Burger, L., Ivanek, R., Lienert, F., Schöler, A., van Nimwegen, E., Wirbelauer, C., Oakeley, E.J., Gaidatzis, D., et al. (2011). DNA-binding factors shape the mouse methylome at distal regulatory regions. Nature *480*, 490–495.

Stein, R., Razin, A., and Cedar, H. (1982). In vitro methylation of the hamster adenine phosphoribosyltransferase gene inhibits its expression in mouse L cells. Proc. Natl. Acad. Sci. U S A *79*, 3418–3422.

Stern, J.L., Paucek, R.D., Huang, F.W., Ghandi, M., Nwumeh, R., Costello, J.C., and Cech, T.R. (2017). Allele-specific DNA methylation and its interplay with repressive histone marks at promoter-mutant TERT genes. Cell Rep. *21*, 3700–3707.

Suzuki, M., Liao, W., Wos, F., Johnston, A.D., DeGrazia, J., Ishii, J., Bloom, T., Zody, M.C., Germer, S., and Greally, J.M. (2018). Whole-genome bisulfite sequencing with improved accuracy and cost. Genome Res. *28*, 1364–1371.

Takashiba, S., Van Dyke, T.E., Amar, S., Murayama, Y., Soskolne, A.W., and Shapira, L. (1999). Differentiation of monocytes to macrophages primes cells for lipopolysaccharide stimulation via accumulation of cytoplasmic nuclear factor kappaB. Infect. Immun. *67*, 5573–5578.

Thurman, R.E., Rynes, E., Humbert, R., Vierstra, J., Maurano, M.T., Haugen, E., Sheffield, N.C., Stergachis, A.B., Wang, H., Vernot, B., et al. (2012). The accessible chromatin landscape of the human genome. Nature *489*, 75–82.

Traore, K., Trush, M.A., George, M., Jr., Spannhake, E.W., Anderson, W., and Asseffa, A. (2005). Signal transduction of phorbol 12-myristate 13-acetate (PMA)-induced growth inhibition of human monocytic leukemia THP-1 cells is reactive oxygen dependent. Leuk. Res. *29*, 863–879.

Tsuchiya, S., Kobayashi, Y., Goto, Y., Okumura, H., Nakae, S., Konno, T., and Tada, K. (1982). Induction of maturation in cultured human monocytic leukemia cells by a phorbol diester. Cancer Res. *42*, 1530–1536.

Vardimon, L., Kressmann, A., Cedar, H., Maechler, M., and Doerfler, W. (1982). Expression of a cloned adenovirus gene is inhibited by in vitro methylation. Proc. Natl. Acad. Sci. U S A *79*, 1073–1077.

Wang, Q., Gu, L., Adey, A., Radlwimmer, B., Wang, W., Hovestadt, V., Bähr, M., Wolf, S., Shendure, J., Eils, R., et al. (2013). Tagmentation-based whole-genome bisulfite sequencing. Nat. Protoc. *8*, 2022–2032.

Wickham, H. (2009). ggplot2: Elegant Graphics for Data Analysis (Springer).

Wu, M., and Gu, L. (2019). TCseq: time course sequencing data analysis. R package version 1.6.1. https://bioconductor.org/packages/release/bioc/html/TCseq.html.

Yu, G., Wang, L.G., Han, Y., and He, Q.Y. (2012). clusterProfiler: an R package for comparing biological themes among gene clusters. OMICS *16*, 284–287.

Yu, G., Wang, L.G., and He, Q.Y. (2015). ChIPseeker: an R/Bioconductor package for ChIP peak annotation, comparison and visualization. Bioinformatics *31*, 2382–2383.

Zentner, G.E., Tesar, P.J., and Scacheri, P.C. (2011). Epigenetic signatures distinguish multiple classes of enhancers with distinct cellular functions. Genome Res. *21*, 1273–1283.

Zhang, Y., Liu, T., Meyer, C.A., Eeckhoute, J., Johnson, D.S., Bernstein, B.E., Nusbaum, C., Myers, R.M., Brown, M., Li, W., and Liu, X.S. (2008). Model-based analysis of ChIP-Seq (MACS). Genome Biol. *9*, R137.

# STAR★METHODS

## KEY RESOURCES TABLE

| REAGENT or RESOURCE | SOURCE | IDENTIFIER |
|---|---|---|
| Bacterial and Virus Strains | | |
| T7 Express *lysY/I$^{q}$* Competent *E. coli* | New England Biolabs | Cat#C3013I |
| Chemicals, Peptides, and Recombinant Proteins | | |
| RPMI Medium 1640 | GIBCO | Cat#11875093 |
| GlutaMAX Supplement | GIBCO | Cat#35050061 |
| Penicillin-Streptomycin (10,000 U/mL) | GIBCO | Cat#15140122 |
| Sodium Pyruvate (100mM) | GIBCO | Cat#11360070 |
| TrypLE Express Enzyme (1X), no phenol red | GIBCO | Cat#12604013 |
| Trypan Blue Stain (0.4%) | GIBCO | Cat#15250061 |
| Fetal Bovine Serum | Peak Serum | Cat#PS-FB1 |
| Dimethyl Sulfoxide | Sigma | Cat#D8418 |
| L-Ascorbic acid 2-phosphate | Sigma | Cat#A8960 |
| Phorbol 12-myristate 13-acetate | Sigma | Cat#P8139 |
| Schneider's Drosophila Medium | GIBCO | Cat#21720001 |
| T4 DNA Polymerase | New England Biolabs | Cat#M0203S |
| Klenow Fragment (3′→5′ exo-) | New England Biolabs | Cat#M0212S |
| Ampligase® Enzyme and Buffer | Lucigen | Cat#A3202K |
| NEBNext® High-Fidelity 2X PCR Master Mix | New England Biolabs | Cat#M0541S |
| KAPA HiFi HotStart Uracil+ ReadyMix (2X) | Roche | Cat#07959052001 |
| TRIzol Reagent | Thermo Fisher Scientific | Cat#15596018 |
| IGEPAL® CA-630 | Sigma | Cat#I8896 |
| Trizma® hydrochloride solution | Sigma | Cat#T2319 |
| Isopropyl-β-D-thiogalactopyranoside (IPTG) (Dioxane-free) | Thermo Fisher Scientific | Cat#BP1755-1 |
| cOmplete™, EDTA-free Protease Inhibitor Cocktail | Sigma | Cat#11873580001 |
| Chitin Resin | New England Biolabs | Cat#S6651S |
| Dimethylformamide | Thermo Fisher Scientific | Cat#D119-1 |
| 5-Methylcytosine dNTP Mix | Zymo Research | Cat#D1030 |
| Critical Commercial Assays | | |
| EZ DNA Methylation-Lightning Kit | Zymo Research | Cat#D5030 |
| SMARTer® Stranded Total RNA Sample Prep Kit - HI Mammalian | Takara Bio USA | Cat#634874 |
| DNA Clean & Concentrator-5 | Zymo Research | Cat#D4004 |
| MycoAlert™ Mycoplasma Detection Kit (25 Tests) | Lonza | Cat#LT07-218 |
| Deposited Data | | |
| ATAC-seq of THP-1 monocytes stimulated with PMA (0hr and 24hr) | This study | GEO: GSE130096 |
| ATAC-Me-seq of THP-1 monocytes stimulated with phorbol 12-myristate 13-acetate (0hr, 0.5hr, 1hr, 2hr, 24hr) | This study | GEO: GSE130096 |
| RNA-seq of mRNA from THP-1 monocytes stimulated with phorbol 12-myristate 13-acetate (0hr, 0.5hr, 1hr, 2hr, 24hr) | This study | GEO: GSE130096 |
| WGBS of THP-1 monocytes stimulated with phorbol 12-myristate 13-acetate (0hr and 24hr) | This study | GEO: GSE130096 |
| H3K27Ac ChIP-seq of phorbol 12-myristate 13-acetate stimulated THP-1 monocytes (0hr and 72hr) | Phanstiel et al., 2017 | GEO: GSE96800 |

(*Continued on next page*)

*Continued*

| REAGENT or RESOURCE | SOURCE | IDENTIFIER |
|---|---|---|
| ATAC-Me-seq of THP-1 monocytes stimulated with phorbol 12-myristate 13-acetate (0hr, 24hr, 48hr, 72hr) and L-Ascorbic acid 2-phosphate treatment (72hr) | This study | GEO: pending |
| Drosophila WGBS comparing DNA library construction methods | This study | GEO: pending |
| Experimental Models: Cell Lines | | |
| THP-1 Monocytes | Gift of Dr. Manuel Ascano Jr., ATCC | Cat#TIB-202 |
| S2 cells | Gift of Dr. Andrea Page-McCaw, ATCC | Cat#CRL-1963 |
| Oligonucleotides | | |
| Oligonucleotides for Tn5 based bisulfite library construction | See Table S2 | N/A |
| Recombinant DNA | | |
| pTXB1-Tn5 Plasmid | Gift of Dr. Rickard Sandberg; Picelli et al., 2014) | Addgene plasmid #60240 |
| Software and Algorithms | | |
| SAMtools | Li et al., 2009 | version 1.5 |
| BEDtools | Quinlan and Hall, 2010 | version 2.26.0 |
| MACS2 | Zhang et al., 2008 | version 2.1 |
| Deeptools | Ramírez et al., 2014 | version 3.1.2 |
| MethPipe | Song et al., 2013 | version 3.4.3 |
| WALT | Chen et al., 2016 | version 1.0 |
| STAR aligner | Dobin et al., 2013 | version 2.6.1a |
| Bowtie2 | Langmead and Salzberg, 2012 | version 2.2.6 |
| DESeq2 | Love et al., 2014 | version 1.18.1 (R version 3.4.3) |
| ChIPseeker | Yu et al., 2015 | version 1.14.2 (R version 3.4.3) |
| ClusterProfiler | Yu et al., 2012 | version 3.6.0 (R version 3.4.3) |
| TCseq | https://bioconductor.org/packages/release/bioc/html/TCseq.html | version 1.1.0 (R version 3.4.3) |
| ggplot2 | Wickham, 2009 | version 3.1.1 (R version 3.5.3) |
| Trimgalore | http://www.bioinformatics.babraham.ac.uk/projects/trim_galore/ | version 0.4.0 |
| pyDNase | Piper et al., 2013 | version 0.3.0 |
| HOMER | Heinz et al., 2010 | version 4.10 |
| Cutadapt | Martin, 2011 | version 1.8.3 |
| Preseq | Daley and Smith, 2013 | version 2.0 |
| Fastqc | https://www.bioinformatics.babraham.ac.uk/projects/fastqc/ | version 0.11.4 |
| Other | | |
| Detailed protocol for ATAC-Me sequencing library construction | This study | Methods S1 |

## LEAD CONTACT AND MATERIALS AVAILABILITY

Inquiries regarding reagents and analyses used in this study should be directed to the lead contact (emily.hodges@vanderbilt.edu). This study did not generate new unique reagents.

## EXPERIMENTAL MODEL AND SUBJECT DETAILS

### THP-1 monocytes

THP-1 cells (gift of Dr. Manuel Ascano Jr., Vanderbilt University) were cultured in RPMI Medium 1640 supplemented with 10% fetal bovine serum, 2mM GlutaMAX, 100 units/mL penicillin, 100 μg/mL streptomycin and 1mM sodium pyruvate (referenced as complete

RPMI medium). Culture conditions were maintained at 5% $CO_2$, 37°C and 80% humidity. During routine culture THP-1 cells were maintained at a density of 0.5-2E6 cells/mL with 50% media change every 72 hours.

### *Drosophila* S2 Cells

S2 cells (gift of Dr. Andrea Page-McCaw, Vanderbilt University) were cultured in Schneider's *Drosophila* Medium supplemented with 10% heat inactivated fetal bovine serum, 100 units/mL penicillin and 100 μg/mL streptomycin. Culture conditions were maintained at 25°C, with atmospheric $CO_2$ and humidity. During routine culture cells were maintained at a density of 2-10E6 cells/mL.

All cell lines have been authenticated by genome sequencing and were regularly screened for mycoplasma contamination using the MycoAlert kit (Lonza).

## METHOD DETAILS

### Cell Treatments

In preparation for the PMA time course, $5x10^6$ THP-1 monocytes were plated in 1mL complete RMPI medium/well of a flat bottom 6-well cell culture treated plate. Differentiation was subsequently induced by addition of 1mL complete RPMI medium supplemented with 200ng PMA for a final PMA concentration of 100ng/mL PMA (162nM). Additions of PMA were temporally staggered to allow for simultaneous collection of time points. THP-1 L-AA-2-P treatment conditions were initially plated identically to PMA only conditions in a final volume of 2mL complete RPMI medium with 100ng/mL PMA. Plated cells were then supplemented with 50mM L-AA-2-P to a final concentration of 350μM. L-AA-2-P was replenished with daily media changes to account for L-AA-2-P degradation over time until harvest at 72hrs. PMA stimulation was withdrawn due to toxicity after 24 hours for extended time points (48hr, 72hr). THP-1 cells were harvested by first collecting non-adherent cells suspended in media followed by a 5 minute incubation with TrypLE Express at 37°C to collect adherent cells. Non-adherent and adherent cells were pooled and pelleted at 4°C, 500 R.C.F for 5 minutes in a 15mL conical tube. After pelleting cells were resuspended in ice cold PBS and counted using an automated cell counter with trypan blue to assess cell viability. Approximately $1x10^6$ cells were reserved for TRIzol RNA extraction, $1x10^6$ cells for ATAC reactions and $2x10^5$ cells for genomic DNA extraction.

### Transposome Preparation

Plasmid (pTXB1-Tn5, gift of Dr. Rickard Sandberg, Karolinska Institutet) for production of Tn5 transposase (Picelli et al., 2014) was transformed into *E. coli* strain C3013 (NEB) according to manufacturer supplied protocol on ampicillin plates. Resulting bacterial colonies were inoculated into 5mL LB + 100μg/mL ampicillin and incubated at 37°C to OD600 = 1.0. 5mL cultures were subsequently used to inoculate 1L LB +100μg/mL ampicillin and grown at 37°C, shaking at 220RPM in baffled flasks until OD600 was approximately 0.70. Cultures were then transferred to an ice water bath and cooled to 15°C. Protein expression was induced by adding IPTG to a final concentration of 250μM followed by incubation at 23°C with shaking at 120RPM for approximately 4hrs or until OD600 = approximately 2.1. Bacteria cultures were harvested by centrifugation at 5,000 RPM (F9-4x1000y rotor), 4°C for 10 min in 1L centrifuge bottles. Supernatants were decanted and pellets stored overnight at −70°C. The following day pellets were thawed and resuspended in 60mL HEGX buffer (20 mM HEPES-KOH at pH 7.2, 0.8 M NaCl, 1 mM EDTA, 10% glycerol, 0.2% Triton X-100) supplemented with Complete EDTA-free protease inhibitor tablet (Roche). The thawed bacterial suspension was cooled on salt-ice to −1°C and subsequently lysed with 8 rounds of sonication for 40 s at 70% duty cycle. During sonication the lysate was cooled repeatedly on salt-ice to avoid warming above 10°C. Lysis progress was monitored by removing 200μL aliquots between rounds of sonication and comparing pellet size after low speed centrifugation at 2000 R.C.F for 1 min. Lysate was then pelleted at 15K RPM (SS-34 rotor), 4°C for 30 min. The pelleted lysate supernatant was cleared of contaminating *E. coli* genomic DNA by drop wise addition of 1.6mL 10% neutralized PEI solution with slow stirring. The PEI lysate solution should begin to turn milky white as the DNA precipitate forms. Lysate was pelleted at 12,000 RPM (SS-34 rotor), 4°C for 10 min. Supernatant was loaded onto a prepared 5mL chitin column at 0.4mL/min flow rate, 4°C. Chitin column was washed with 300mL HEGX buffer at a flow rate of 0.4mL/min. Tn5 transposase was eluted by the addition of 14mL HEGX + 100mM DTT to the column, followed by a 48hr incubation at 4°C to induce cleavage from the column. Tn5 transposase was collected from the column in 1mL fractions and subsequently analyzed for protein concentration. Fractions with the highest protein concentration were pooled and dialyzed twice with 1L of 2x dialysis buffer (100mM HEPES, pH 7.2, 0.2M NaCl, 0.2mM EDTA, 2mM DTT, 0.2% TX100, 20% Glycerol). Dialyzed protein was concentrated with Amicon Ultracel 30 centrifugal filters (Millipore) in multiple rounds of centrifugation at 3000 RCF, 4°C for 20 min with intermittent mixing until a final OD280 of at least 3.0. Purified Tn5 transposase was aliquoted and stored at −20°C after the addition of 1 volume 100% glycerol.

Standard ATAC transposome adapters were prepared by annealing two oligo mixes in separate PCR tubes (Mix A: 5μl 100μM Tn5MEREV oligo, 5μl 100μM Tn51 oligo, 40μL nuclease free water; Mix B: 5μl 100μM Tn5MEREV oligo, 5μl 100μM Tn5_2_ME_Comp oligo, 40μL nuclease free water). Oligo mix A and B were both incubated in a PCR thermocycler as follows: 95°C for 3 minutes, 65°C for 3 minutes, ramp down to 24°C at a rate of −1°C/second, hold at 24°C. After annealing, oligo mix A and B were combined along with 100μL glycerol to create a 5μM, 50% glycerol adaptor mixture. Transposomes were assembled by mixing equal parts purified Tn5 transposase enzyme and adaptor mixture followed by a 25°C incubation for 60 min.

ATAC-Me and T-WGBS transposome adapters were prepared by annealing the oligonucleotides in PCR tubes (10μl 100μM Tn5mC-Apt1 oligo, 10μl 100μM Tn5mC1.1-A1block oligo, 80μL nuclease free water). Oligos were incubated in a PCR thermocycler

as follows: 95°C for 3 minutes, 65°C for 3 minutes, ramp down to 24°C at a rate of −1°C/second, hold at 24°C. After annealing oligos were combined along with 100μL glycerol to create a 5μM, 50% glycerol adaptor mixture. Transposomes were assembled by mixing equal parts purified Tn5 transposase enzyme and adaptor mixture followed by a 25°C incubation for 60 min.

Extension based T-WGBS transposome adapters (Spektor et al., 2019) were prepared by annealing two oligo mixes in separate PCR tubes (Mix A: 5μl 100μM Tn5MEREV oligo, 5μl 100μM Tn5mC-Apt1 oligo, 40μL nuclease free water; Mix B: 5μl 100μM Tn5MEREV oligo, 5μl 100μM Meth_Tn5_2_ME_comp oligo, 40μL nuclease free water). Oligo mix A and B were both incubated in a PCR thermocycler as follows: 95°C for 3 minutes, 65°C for 3 minutes, ramp down to 24°C at a rate of −1°C/second, hold at 24°C. After annealing, oligo mix A and B were combined along with 100μL glycerol to create a 5μM, 50% glycerol adaptor mixture. Transposomes were assembled by mixing equal parts purified Tn5 transposase enzyme and adaptor mixture followed by a 25°C incubation for 60 min.

All oligonucleotides utilized for transposome assembly are provided in Table S2.

## ATAC-seq

ATAC-seq libraries were prepared similarly to previously reported methods (Buenrostro et al., 2013). Harvested THP-1 cells were centrifuged at 4°C, 500 R.C.F for 5 min and subsequently resuspended in 1mL ice cold PBS. Resuspended cells were counted and assayed for cell viability with trypan blue using an automated cell counter. Cell viability > 80% was required to proceed with library preparation. Cell suspension volume corresponding to $2x10^5$ THP1 cells was pipetted into a 1.5mL eppendorf tube and pelleted at 4°C, 500 R.C.F for 5 min. Supernatant was aspirated and the cell pellet resuspended in 150μL cold ATAC lysis buffer (10mM Tris-HCl pH 7.4, 10mM NaCl, 3mM $MgCl_2$, 0.1% IGEPAL-630). This suspension was agitated by gently pipetting up/down with a 200μL micropipette tip 10 times. Subsequently, this suspension was pelleted at 4°C, 500 R.C.F for 10 minutes. Supernatant was discarded and nuclei pellet immediately resuspended in 190μL transposition reaction mix (10mM Tris-HCl pH 7.5, 5mM $MgCl_2$, 10% Dimethylformamide) by pipetting up/down with a 200μL micropipette tip 3 times. 10μL of pre-assembled Tn5 transposome with standard ATAC adapters was added. Tubes were gently agitated to mix all components and incubated at 37°C, 30 minutes, 700RPM in an Eppendorf Thermomixer. ATAC reactions were terminated by adding 1mL Zymo DNA binding buffer and vortexing. Reactions were purified according to manufacturer instructions in a DNA Clean and Concentrator-5 kit (Zymo) and eluted in 25μL nuclease free water. Eluted ATAC DNA was amplified and barcoded in 50μL PCR reactions (25μL 2x NEBNext High-Fidelity PCR Master Mix, 20μL eluted ATAC DNA, 2.5μL 10μM i5 index primer, 2.5μL 10μM i7 index primer) with the following PCR thermocycler program: 72°C 5 min; 98°C 30 s; 8 cycles of 98°C 10 s, 62°C 30 s, 72°C 30 s; final extension 72°C 5 min; hold at 12°C. Post-amplification PCR reactions were cleaned and concentrated with a Zymo DNA Clean and Concentrator-5 column kit. DNA was eluted in 22μL nuclease free $H_2O$. Preliminary library analysis for concentration and size distribution was performed using an Agilent 2200 TapeStation with a D5000 screentape. ATAC-seq DNA libraries were sequenced using 2x75bp paired-end reads on the NextSeq500 instrument.

## ATAC-Me

Harvested THP-1 cells were centrifuged at 4°C, 500 R.C.F for 5 min and subsequently resuspended in 1mL ice cold PBS. Resuspended cells were counted and assayed for cell viability with trypan blue using an automated cell counter. Cell viability > 80% was required to proceed with library preparation. Cell suspension volume corresponding to $2x10^5$ THP1 cells was pipetted into a 1.5mL eppendorf tube and pelleted at 4°C, 500 R.C.F for 5 min. Supernatant was aspirated and the cell pellet resuspended in 150μL cold ATAC lysis buffer (10mM Tris-HCl pH 7.4, 10mM NaCl, 3mM $MgCl_2$, 0.1% IGEPAL-630). This suspension was agitated by gently pipetting up/down with a 200μL micropipette tip 10 times. The suspension was pelleted at 4°C, 500 R.C.F for 10 minutes. Supernatant was discarded and nuclei pellet immediately resuspended in 190μL transposition reaction mix (10mM Tris-HCl pH 7.5, 5mM $MgCl_2$, 10% Dimethylformamide) by pipetting up/down with a 200μL micropipette tip 3 times. 10μL of pre-assembled Tn5 transposome (containing methylated adaptors) was added. Tubes were gently agitated and incubated at 37°C, 30 minutes, 700RPM in an Eppendorf Thermomixer. ATAC-Me reactions were terminated by adding 1mL Zymo DNA binding buffer and vortexing. Reactions were purified according to manufacturer instructions in a DNA Clean and Concentrator-5 kit (Zymo) and eluted in 13μL nuclease free water.

DNA eluate was used as input into the gap repair reaction (11μL ATAC-Me DNA eluate, 2μL 10μM Tn5mC-Repl01 oligo, 2μL 10x ampligase buffer, 2μL dNTPs 2.5mM each). This gap repair reaction was assembled in a PCR tube and incubated as follows in a PCR thermocycler: 50°C for 1 minute, 45°C for 10 minutes, ramp down to 37°C at a rate of −0.1°C/second, hold at 37°C. Once reaching 37°C, 1μL T4 DNA polymerase and 2.5μL ampligase were added separately without removing the tube from the thermocycler. After final addition of enzymes, the reaction was mixed by pipetting up/down with a 20μL micropipette tip without removing tube from the thermocycler. The gap repair reaction was incubated as follows: 37°C for 30 minutes, hold at 4°C. 2μL of the gap repair reaction was reserved for a test PCR amplification to confirm successful ATAC nucleosomal laddering. 2μL of 250mM EDTA (pH = 8.0) was added to stop the gap repair reaction. Gap repaired ATAC-Me material was bisulfite converted according to manufacturer instructions using the Zymo Lightning EZ DNA Methylation-Lightning Kit (cat no D5030) with slight modification. 20μL gap repaired DNA and 130μL CT conversion reagent were mixed and split between three PCR tubes, 50μL/tube. Bisulfite conversion reactions were then incubated in PCR tubes as follows: 98°C for 8 minutes, 54°C for 60 minutes, hold at 4°C. The three bisulfite conversion reactions were re-pooled into a single tube. Final purification/desulfonation was performed as directed by the kit manufacturer manual instructions. Final

elution was in 25μL of M-elution buffer supplied by the kit. Eluted ATAC-Me DNA was amplified and barcoded in 50μL PCR reactions (25μL 2x KAPA HiFi HotStart Uracil+ ReadyMix, 20μL eluted ATAC-Me DNA, 1.5μL 10μM i5 index primer, 1.5μL 10μM i7 index primer) with the following PCR thermocycler program: 98°C 45 s; 10 cycles of 98°C 15 s, 62°C 30 s, 72°C 30 s; final extension 72°C 2 min; hold at 12°C. Post-amplification PCR reactions were cleaned and concentrated with a Zymo DNA Clean and Concentrator-5 column kit. Elution was in 22μL nuclease free $H_2O$. Preliminary library analysis for concentration and size distribution was performed using an Agilent 2200 TapeStation with a D5000 screentape. ATAC-Me DNA libraries were sequenced using 2x150bp paired-end reads on the HiSeq4000 and NovaSeq6000 instruments.

### THP-1 T-WGBS

THP-1 T-WGBS libraries were prepared similarly to previously reported methods (Adey and Shendure, 2012; Wang et al., 2013). Genomic DNA purified from THP-1 cells was diluted in a 50μL tagmentation reaction (100ng genomic DNA, 10mM Tris-HCl pH 7.5, 5mM $MgCl_2$, 10% Dimethylformamide). 2.5μL of transposome assembled with T-WGBS adapters was added and the reaction incubated at 55°C for 8 min in a PCR thermocycler. Tagmentation reactions were immediately stopped with the addition of 250μL Zymo DNA binding buffer from the DNA Clean & Concentrator-5 kit (Zymo). Reactions were then purified according to manufacturer instructions in a DNA Clean and Concentrator-5 kit (Zymo) and eluted in 15μL nuclease free water. DNA eluate was used as input into the gap repair reaction (11μL ATAC-Me DNA eluate, 2μL 10μM Tn5mC-Repl01 oligo, 2μL 10x ampligase buffer, 2μL dNTPs 2.5mM each). This gap repair reaction was assembled in a PCR tube and incubated as follows in a PCR thermocycler: 50°C for 1 minute, 45°C for 10 minutes, ramp down to 37°C at a rate of −0.1°C/second, hold at 37°C. Upon reaching 37°C, 1μL T4 DNA polymerase and 2.5μL ampligase were added separately without removing the tube from the thermocycler. The reaction was mixed by pipetting up/down with a 20μL micropipette tip without removal from the thermocycler. The gap repair reaction was subsequently incubated as follows: 37°C for 30 minutes, hold at 4°C. 2μL of the gap repair reaction was reserved for a test PCR amplification for troubleshooting. 2μL of 250mM EDTA (pH = 8.0) was added to stop the reaction. Gap repaired, tagmented DNA was subsequently bisulfite converted according to manufacturer instructions using the Lightning EZ DNA Methylation-Lightning Kit (Zymo) with slight modification. 20μL gap repaired DNA and 130μL CT conversion reagent were mixed and split between three PCR tubes, 50μL/tube. Bisulfite conversion reactions were then incubated in PCR tubes as follows: 98°C for 8 minutes, 54°C for 60 minutes, hold at 4°C. The three bisulfite conversion reactions were re-pooled into a single tube. Final purification/desulfonation was performed as directed by the kit manufacturer manual instructions. Final elution was in 25μL of M-elution buffer supplied by the kit. Eluted bisulfite converted DNA was amplified and barcoded in 50μL PCR reactions (25μL 2x KAPA HiFi HotStart Uracil+ ReadyMix, 20μL eluted ATAC-Me DNA, 1.5μL 10μM i5 index primer, 1.5μL 10μM i7 index primer) with the following PCR thermocycler program: 98°C 45 s; 8 cycles of 98°C 15 s, 62°C 30 s, 72°C 30 s; final extension 72°C 2 min; hold at 12°C. Post-amplification PCR reactions were cleaned and concentrated in a DNA Clean and Concentrator-5 kit (Zymo). Elution was in 22μL nuclease free water. Preliminary library analysis for concentration and size distribution was performed using an Agilent 2200 TapeStation with a D5000 screentape. THP-1 T-WGBS DNA libraries were sequenced using 2x150bp paired-end reads on the HiSeqX instrument.

### *Drosophila* S2 cell T-WGBS

*Drosophila* S2 cell T-WGBS libraries were prepared similarly to previously reported methods (Lu et al., 2015; Spektor et al., 2019; Suzuki et al., 2018). Genomic DNA purified from *Drosophila* S2 cells was diluted in a 50μL tagmentation reaction (100ng genomic DNA, 10mM Tris-HCl pH 7.5, 5mM $MgCl_2$, 10% Dimethylformamide). 2.5μL of transposome assembled with T-WGBS adapters was added and the reaction incubated at 55°C for 8 min in a PCR thermocycler. Tagmentation reactions were immediately halted with the addition of 250μL Zymo DNA binding buffer from the DNA Clean & Concentrator-5 kit (Zymo). Reactions were then purified according to manufacturer instruction in a DNA Clean and Concentrator-5 kit (Zymo) and eluted in 15μL nuclease free water. Eluted DNA was subsequently end-repaired with either Klenow exo- polymerase (NEB) or T4 DNA polymerase (NEB). Klenow extension based libraries were end-repaired by Klenow exo- repair mix (2μL 10x NEBuffer 2.0, 5 units Klenow exo- [NEB], 4μL 2.5mM each 5-methyl-dCTP substituted dNTP mix, 13.5μL eluted tagmented DNA). Klenow repair reactions were incubated at 37°C, 30 minutes followed by adding 2μL 250mM EDTA to terminate the reaction. T4 polymerase extension based libraries were end repaired by T4 polymerase repair mix (2μL 10x NEBuffer 2.1, 2μL 2.5mM each 5-methyl-dCTP substituted dNTP mix, 11μL eluted tagmented DNA). T4 polymerase repair mixture was incubated as follows: 50°C, 1 min; hold at 37°C; add 1μL T4 polymerase, 3000 units/mL (NEB); 37°C, 5 min. T4 polymerase repair reaction was subsequently terminated by adding 2μL 250mM EDTA. Klenow or T4 DNA polymerase end-repaired DNA was bisulfite converted, PCR amplified and sequenced as described above.

### RNA-seq

RNA from approximately $1x10^6$ THP-1 cells was harvested from each PMA stimulation time point by pelleting cells at 4°C, 500 R.C.F for 5 minutes. After removal of supernatant, cell pellet was homogenized with 1mL of TRIzol Reagent by repeatedly pipetting up/down with a 1mL micropipette tip. RNA was purified from Trizol homogenate according to recommended manufacturer instructions. RNA-seq libraries were prepared using the SMARTer® Stranded Total RNA Sample Prep Kit (Takara Bio). RNA-seq libraries were sequenced using 2x100bp paired-end reads on the NovaSeq6000 instrument.

### Sequencing Library Processing

All sequencing library reads were trimmed of adapters using TrimGalore script wrapper for Cutadapt (Martin, 2011) and FastQC. Standard ATAC and ATAC-Me/WGBS reads were mapped with Bowtie2 (Langmead and Salzberg, 2012) or WALT (Chen et al., 2016), respectively, to the hg19 genome assembly (Lander et al., 2001). Methylation analysis of ATAC-Me and WGBS reads was performed using the MethPipe suite of tools (Song et al., 2013). Preseq (Daley and Smith, 2013) was used to compare library complexity across protocols. RNA libraries were mapped with the STAR mapper (Dobin et al., 2013) and analyzed for differential RNA expression using DESeq2 (Love et al., 2014). Regions enriched for chromatin accessibility in standard ATAC and ATAC-Me data were identified using the MACS2 (Zhang et al., 2008) peak caller suite of tools. Regions dynamic for chromatin accessibility were identified with the TCseq R-package (Wu and Gu, 2019). HOMER was used for all transcription factor motif analysis of dynamic or static chromatin accessible regions. Annotation and gene association for dynamic and static chromatin accessible regions was performed with the ChIPseeker (Yu et al., 2015) and ClusterProfiler (Yu et al., 2012) R-packages. *De-novo* footprint analysis by identifying ATAC-seq read signal depressions was performed using the Wellington footprinting algorithm (Piper et al., 2013). Dual analysis of footprint depth and flanking accessibility at pre-identified transcription factor DNA sequence motifs was performed using the bagfootr R-package (Baek et al., 2017). The samtools (Li et al., 2009), bedtools (Quinlan and Hall, 2010) and deeptools (Ramírez et al., 2014) suites of tools were used to aid in data manipulation and visualization.

## QUANTIFICATION AND STATISTICAL ANALYSIS

Chromatin accessibility peaks were initially selected for analysis based upon filtering of the Benjamini-Hochberg corrected p value (q-value) reported by the MACS2 peak-calling algorithm (corr. p value < $1x10^{-10}$). Differentially chromatin accessible genomic loci across the time course were selected from FDR corrected p values produced by the likelihood ratio test implemented in the TCseq R-package (corr. p value < $5x10^{-3}$). Differentially expressed genes across the time course were selected from corrected p values produced by the likelihood ratio test implemented in the DESeq2 R-package (corr. p value < $5x10^{-3}$). Statistical analyses were performed within the R computing environment and visualized with ggplot2 (Wickham, 2009). Details of statistical analyses can found in figure legends and on our Github page (see below).

## DATA AND CODE AVAILABILITY

Datasets utilized in this study may be accessed at GEO: GSE130096 and GEO: GSE96800.

Detailed code and workflows associated with main figures may be accessed at: https://github.com/HodgesGenomicsLab/ATAC-Me

## ADDITIONAL RESOURCES

A detailed step-by-step ATAC-Me sequencing library construction protocol is available in Methods S1.